Seismic profiling in downtown Salt Lake City: Mapping the Wasatch fault with seismic velocity and reflection methods from a land streamer

Project Award Number: # G17AP00052

Award Dates: May 2017 through April 2018

Submission date: July 31, 2018

Project dates: April 15, 2017 through April 14, 2018

Lee M. Liberty

James St. Clair

Gabriel Gribler

Department of Geosciences

Boise State University

Boise, Idaho 83725-1536

Phone: 208-426-1419

lliberty@boisestate.edu

http://cgiss.boisestate.edu/~lml

Research supported by the U.S. Geological Survey (USGS), Department of the Interior, under USGS award number G17AP00052. The views and conclusions contained in this document are those of the authors and should not be interpreted as necessarily representing the official policies, either expressed or implied, of the U.S. Government.

Contents

Abstract

We acquired 35 km of new seismic land streamer data over two field seasons (and two NEHRP awards) that reveal a complex pattern of faulting, folding and shallow deformation within overlapping faults of the Wasatch fault zone beneath downtown Salt Lake City (SLC), Utah. We acquired new data along heavily trafficked city streets using a contact coupled seismic system towed behind a truck-mounted accelerated weight drop source. These data provide the first images of earthquake induced liquefaction and faults that connect the East Bench and Warm Springs segments of the Wasatch fault beneath the dense SLC urban corridor. Lateral spread deposits have been identified from trench studies, and here we map these regions using Rayleigh wave seismic signals to determine that these deposits are rooted in active faults. We find soft deposits beneath much of downtown, leading to high site amplification potential during ground shaking. Seismic reflection images show folding and faulting beneath lateral spread deposits and between mapped strands of the East Bench and Warm Springs faults, implying differential fault slip between faults. This zone of distributed faulting extends to within a few meters of the surface, and a dominant component of faulting trends about N20W to connect East Bench and Warm Springs fault systems. We conclude that latest Pleistocene or Holocene faults extend beneath downtown SLC. Shallow faults, high liquefaction susceptibility and high site amplification potential beneath downtown SLC raises earthquake hazards for the Wasatch front urban corridor by reducing the magnitude where damage from earthquakes can occur. Products from this study include Vp, Vs, Vp/Vs ratios, and reflection profiles; Vs30 site amplification map; Vs30 comparisons to lithology, slope and elevation; distributions of colluvium and water table depth estimates for Salt Lake City.

Introduction

The active, 343-km-long Wasatch fault zone (WFZ) defines the eastern boundary of the Basin and Range Province in central Utah (Figure 1). The urbanized portion of the WFZ is composed of six tectonic segments with a complex earthquake record (summarized in DuRoss et al., 2016). These faults have evidence for at least 24 large-magnitude earthquakes since about 7 ka. The segments range in length from 35 km to 59 km and are each considered individually capable of generating large magnitude (M ~7) surface-rupturing earthquakes. The 35 km long Salt Lake City (SLC) segment of the WFZ consists of three 8-20 km long en echelon faults; the Warm Springs, East Bench and Cottonwood faults (Bruhn et al., 1992; Personious and Scott, 1992). A major earthquake initiating on any one of these faults will produce significant ground amplification by low-velocity sediments that lie below the Salt Lake valley (e.g., Roten et al., 2011). Where these faults surface and how these fault segments interact are critical components to estimate earthquake magnitude scaling and ground displacements (e.g., Petersen et al., 2014). How earthquake ruptures along these faults interact with shallow soft soils beneath the million plus SLC population are critical to site response and liquefaction susceptibility assessments. Constraining these parameters is the focus of this study.

While the 50-70 degree west-dipping Warm Spring fault (WSF) and Cottonwood fault appear as prominent topographic scarps that separate the ~3 km deep Salt Lake basin from the Wasatch Range to the east (Hill et al., 1990; Bruhn et al., 1992; Figure 2), the East Bench fault (EBF) forms a prominent intrabasin fault scarp with little known about subsurface fault geometry or connectivity with adjacent fault segments. The 2-3 km left step between the EBF and the WSF lies beneath the most densely populated portions of SLC, and the slip distribution between these faults is unclear. The west-dipping normal faults of the Wasatch Front separate the ~3 km deep Salt Lake basin from the Wasatch Range to the east (Figure 1). East-dipping antithetic faults, located approximately 5-10 km west of the SLC faults, either control the western Salt Lake basin margin or bisect the basin. These faults comprise the West Valley fault system.

The latest earthquakes on the SLC segment are estimated at about 1.3 ka for the southernmost Cottonwood fault and about 4 ka for the left stepping EBF (DuRoss and Hylland, 2015). The latest earthquake timing on the EBF was from the Penrose trench (DuRoss et al., 2014), located at the very northern end of the mapped fault (Figure 1) where latest Pleistocene and Holocene vertical slip rates are estimated at 0.5–0.9 mm/yr or a vertical displacement of 1.0–1.4 m per-event. In contrast, the Dresden Place trench, located approximately two km to the southwest, revealed about 7 m of deformation in 20-30 ka Lake Bonneville deposits (Machette et al., 1992; Figure 1), or about 0.2-0.35 mm/yr. Detailed paleoseismic earthquake timing for the WSF is lacking, but one trench (Washington Elementary; Figure 1) documented 12 m of displacement since about 15 ka (Robison and Burr, 1991; DuRoss and Hylland, 2015) or a slip rate of about 0.8 mm/year. Because of the left step and possible overlap of the Warm Springs and EBFs at this latitude, DuRoss and Hylland (2015) recognized the paleoseismic record may be incomplete. While lateral steps can be either persistent or non-persistent earthquake barriers, dePolo et al (1989; 1991) found many examples where echelon steps in a fault failed to stop propagating ruptures. Armstrong et al. (2004) placed exhumation rates for the past 5Ma for most of the Wasatch fault at 0.2-

0.4 mm/yr, but portions of the SLC segment show exhumation rates as high as 0.8–1.2 mm/yr (Ehlers et al., 2003). This suggests that along strike variations in slip may be considerable and a detailed understanding of active faults is critical for hazards assessments.

Circumstantial evidence to extend the WSF farther south beyond its topographic expression, to overlap with the EBF, lies at the Salt Palace Convention Center (Figure 1). Here, construction excavations and exploratory trenches revealed complex faulting within the final transgressive phase of Bonneville lake deposits about 11-15 ka (Simon-Bymaster, 1999; Simon and Shlemon, 1999). While others have argued that the faults could have formed from liquefaction induced lateral spread that are mapped in a few locations throughout downtown SLC (Kleinfelder, Inc., 1999; Korbay and McCormick, 1999; Figure 1), a study of eight cone-penetrometer (CPT) soundings about 400 m farther south provided evidence for about 9 m of vertical offset in 20-30 ka Lake Bonneville sediments (Leeflang, 2008; Figure 3) This estimated offset results in a slip rate of about 0.4-0.6 mm/yr, or about half the estimated slip from the Washington school trench approximately 1.5 km to the north and similar to slip rates within the Dresden trenches to the east (Figure 3).

In this study, we first describe the Salt Lake basin through gravity models, geologic, and paleoseismic studies. We then describe our seismic land streamer campaign and results. New seismic data collected as part of this study reveal structural and stratigraphic controls beneath downtown SLC to catalog the distribution of late Pleistocene or Holocene faults. Additionally, the distribution of lake deposits, alluvium, and Tertiary rocks are extracted from seismic properties and place key constraints on earthquake site amplification, the distribution of liquefaction induced lateral spread deposits, and highlight the potential for liquefaction within the downtown corridor. Although the seismic land streamer approach that utilize contact coupled geophones is not new (Van der Veen and Green, 1998; Van der Veen et al., 2001), our integrated surface and body wave analysis along a grid of city streets is novel. This low cost imaging approach provides new opportunities to assess geologic hazards, map subsurface geology and groundwater resources where population and infrastructure are most vulnerable.

Salt Lake basin

The Salt Lake basin is bound by the Wasatch Mountains to the east and the Oquirrh Mountains to the west (Figure 1). These ranges contain Precambrian quartzites, Paleozoic and Mesozoic limestones, and Tertiary volcanic and plutonic rocks (Davis, 1983). Within the basin, three stratigraphic boundaries have been identified and used to estimate earthquake site response for the SLC metropolitan area (e.g., Hill et al., 1990; Bruhn et al., 1992; Magistrale et al., 2006; Roten et al., 2011). Here, we summarize layer properties within the Salt Lake basin from previous studies to relate to our seismic results. We then examine changes in basin geometry across the Warm Springs and East Bench segments of the Wasatch fault to explore fault interactions and characteristics.

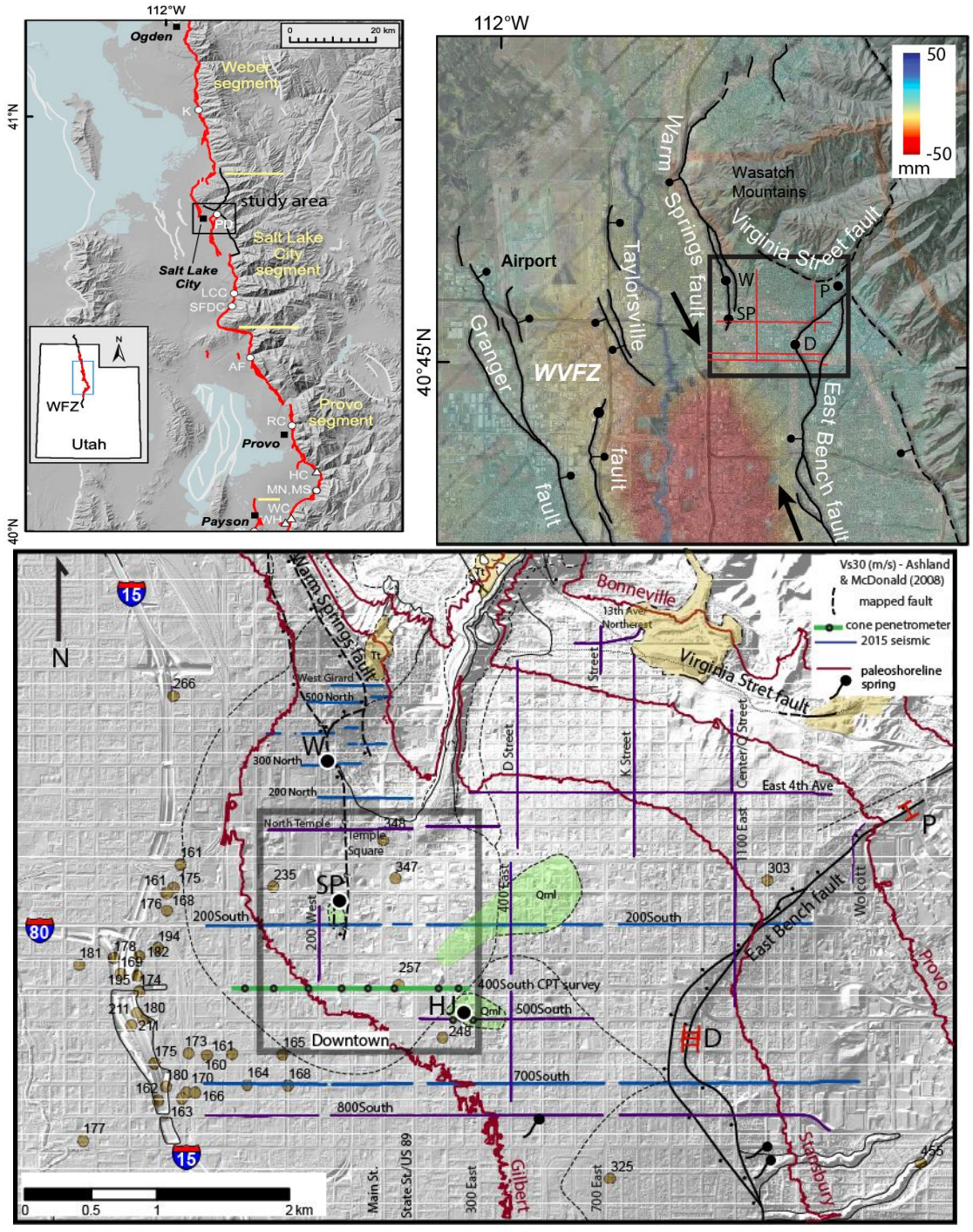

Figure 1. (left) Active faults along Wasatch front in central Utah (from DuRoss et al., 2016). (right) fault and subsidence map of Hu et al (2018). Note the N20W subsidence boundary (arrows) along strike of the WSF. (bottom) Lidar-derived study area map showing faults (black lines), paleoshorelines (red lines), seismic profiles, groundwater springs, and select geologic units including lateral spread deposits (Qml) and Tertiary sedimentary and volcanic rocks (yellow). Washington Elementary trench (W), Salt Palace (SP), Dresden Place trenches (D), Penrose trench (P), Hall of Justice (HJ). Brown circles with numbers represent Vs30 borehole measurements from McDonald and Ashland (2008).

The geometry of the Salt Lake basin has been previously characterized by seismic and gravity data. P-wave seismic velocities (Vp) for the presumed basement rocks, here termed Unit IV, are estimated at 6,000 m/s (Bashore, 1982). Hill et al., (1990) assigned a density of 2.75 g/cc for this lowest layer and identified a maximum thickness of about 3 km along a seismic profile located about 5 km north of downtown Salt Lake City (Figure 2). Bashore (1982) assumed a unit IV Vp/Vs ratio of 1.72 to assign a shear wave velocity (Vs) of 3,460 m/s for basement rocks. These velocity estimates are similar to US Array-derived Vp crustal average estimates of 6,276 m/s and Vs estimate of 3,922 m/s for nearby station NOQ (Vp/Vs = 1.6) (IRIS DMC, 2010).

Above basement, borehole sonic and density logs suggest an average Vp measurement of 5,000 m/s and a bulk density of 2.65 g/cc for consolidated Paleozoic basin sedimentary rocks (Hill, 1990). Hill (1988) defined a prominent reflector as the boundary between Paleozoic sedimentary rocks and overlying Tertiary strata, here termed Unit II (Figure 3). This interpretation is consistent with measured borehole Vp values of 2,450 m/s and bulk density estimates of 2.2 g/cc (Hill, 1990). Using a Vp/Vs ratio of 1.9 for these medium porosity sedimentary rocks (Lee, 2003), we assume a Vs of about 1,290 m/s for Unit II. Stephenson et al (2012) measured velocities of 2,800 m/s for Tertiary strata to the south of SLC.

Of relevance to our seismic study, one of the largest and best studied paleolakes in the world is Lake Bonneville that lasted from about 30-10 ka (e.g., Oviatt et al., 1992; Oviatt, 2015). This paleolake is the predecessor to the Great Salt Lake, filled the Salt Lake basin, and consisted of transgressive and regressive phases that extended to an elevation of 1551 m for the 18 ka Bonneville shoreline (Figure 1). This highstand defines the limits of the Salt Lake basin (Figure 1). The final regressive phase of Lake Bonneville, termed the Provo phase, is estimated at 15-18 ka and extended to about 1445 m elevation. At about 13 ka, Lake Bonneville regressed to altitudes of the modern Great Salt Lake (about 1280 m), then transgressed to a maximum altitude of 1295 to 1297 m about 11 ka. This final lake transgression is referred to as the Gilbert episode. Personious and Scott (1992) documented a general increase in surficial deposit ages across our study area where modern stream alluvium lies beneath the southwestern limits (Figure 2). Lake strata transition from Holocene to latest Pleistocene to late Pleistocene from west to east. Between one to ten meters of fan alluvium lies upon the lacustrine deposits across north and eastern portions of our study area (Figure 3). Where we identify tectonic offsets or deformation across the youngest Bonneville strata, we infer active tectonics.

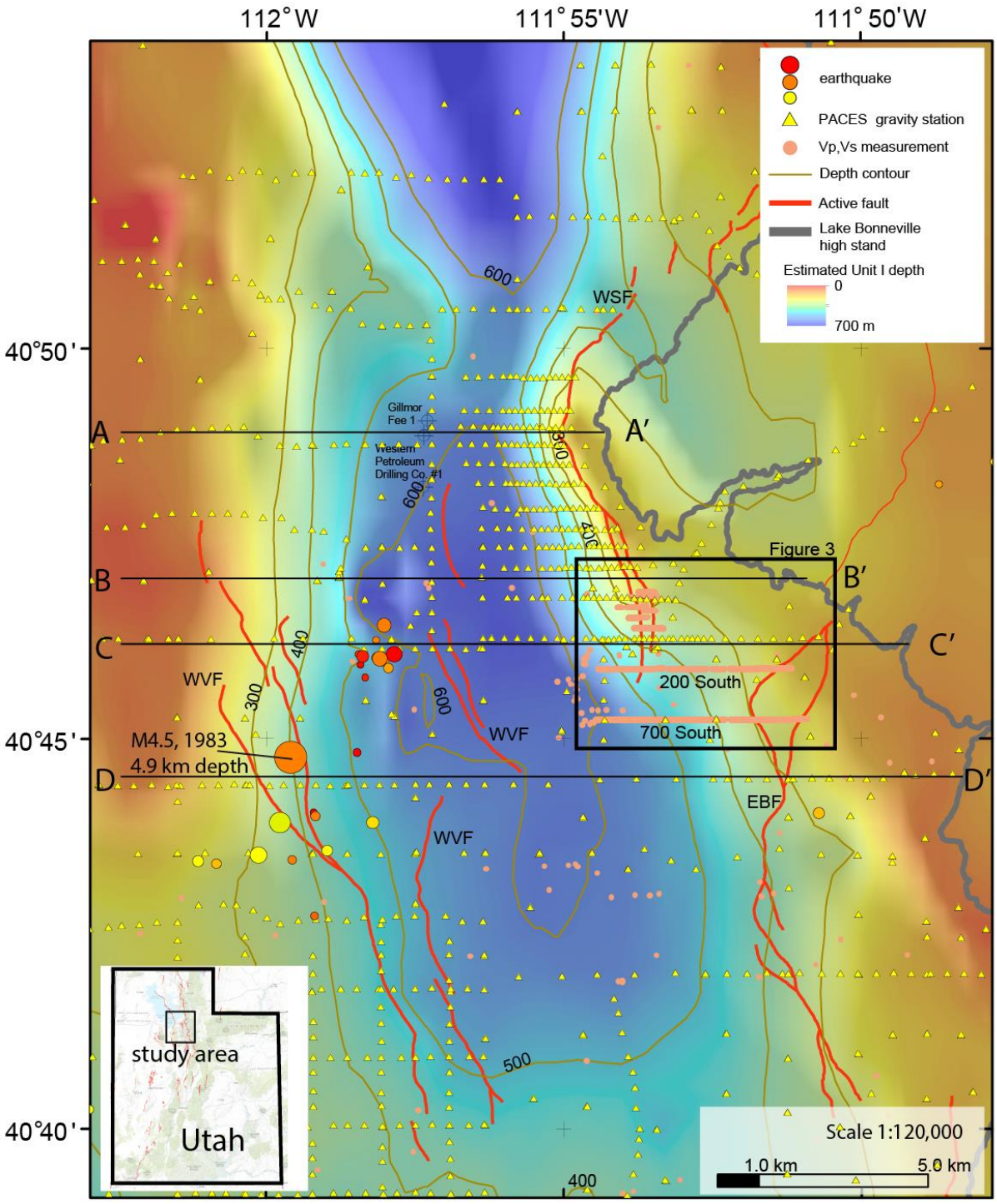

Figure 2. Shaded contour map for gravity-derived depth to base of Unit RI or top of Tertiary strata derived from gravity model. Gravity stations appear as yellow circles and recorded earthquakes are colored by depth (shallower depths are hotter colors). WSF = Warm Springs fault, EBF = East Bench fault, WVF = West Valley fault). Seismic profile R-1 parallels profile A-A'. 2015 seismic profiles are shown on map as tan lines. Gray line represents the eastern extent of Lake Bonneville.

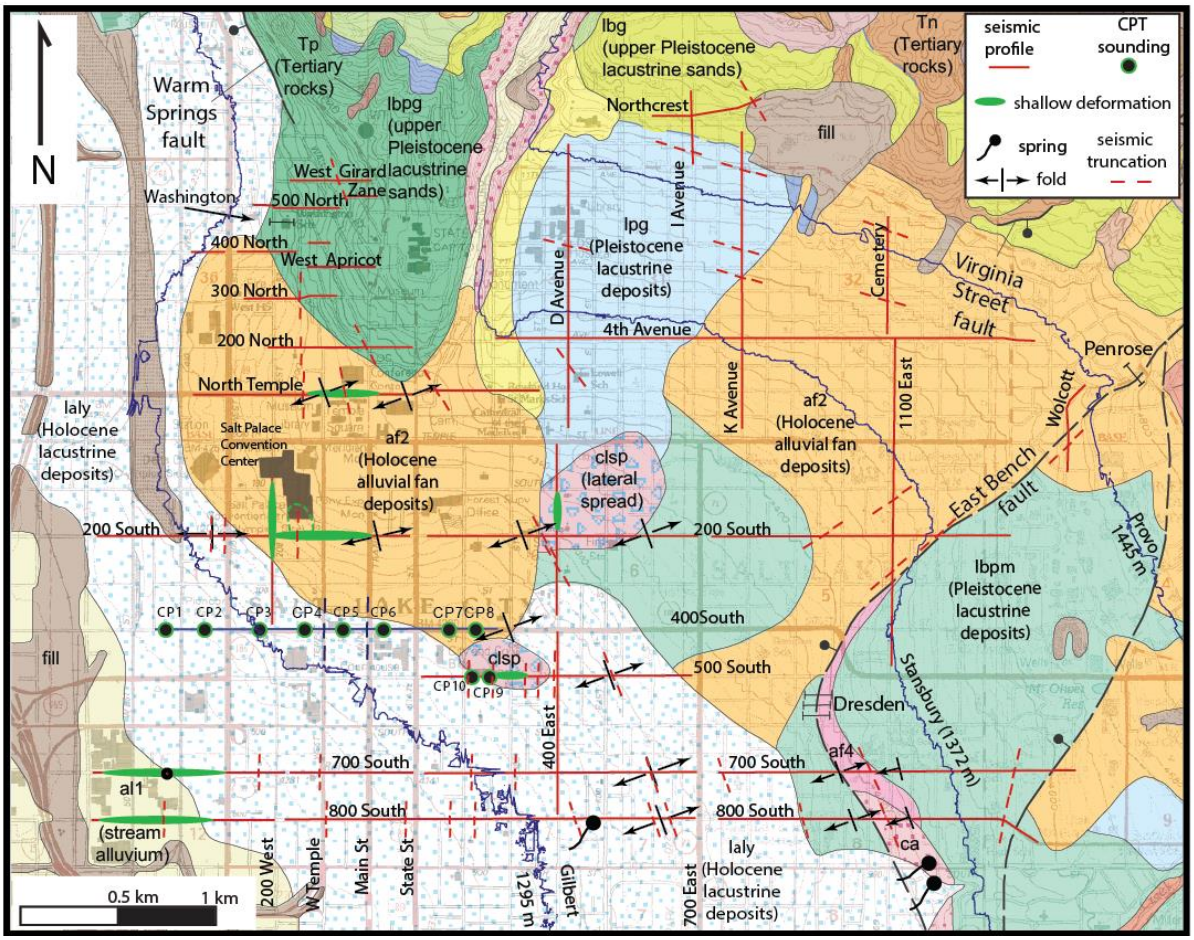

Figure 3. Geologic map of Personious and Scott (1992) with seismic profile locations (red lines) and simplified interpretations from this study. CPT soundings along 400 South and 500 South (black dots). Red dashes represent lateral terminations in seismic reflection refraction profiles and fold apexes (black arrows) are derived from reflection results. Green ellipses represent lateral spread deposits mapped from Rayleigh waves.

Gravity derived basin model

Similar to the Magistrale et al. (2006) and Roten et al (2011) approach to construct a community velocity model for the SLC area, we utilize gravity data to derive boundary depths for the four simplified lithologic units. We use data compiled by and the Pan American Center for Earth and Environmental Sciences (http://gis.utep.edu/subpages/GMData.html) where gravity measurements were obtained with a North American Datum of 1927 (NAD 27) and were terrain corrected using a USGS-derived digital elevation model. We use the complete Bouguer anomaly data provided by the PACES database where depths to key geologic boundaries were constrained by active source seismic data and borehole geophysical measurements (Figure 2). Constraints for gravity models were derived from seismic reflection profile R-11 (Hill, 1988; Radkins et al., 1989) that is located along our northern profile A-A'

(Figure 4), from the refraction results of Bashore (1982) that crosses the southern margins of the Salt Lake basin (about latitude 40.6 North), and from density and seismic velocity logs from nearby oil and gas wells (http://mapserv.utah.gov/oilgasmining/) that are located near the northern profile and are also summarized in Hill et al. (1990). We invert for basin geometry assuming a four-layer density model. We then extract profiles along densely sampled transects to the elevation of the Bonneville high stand.

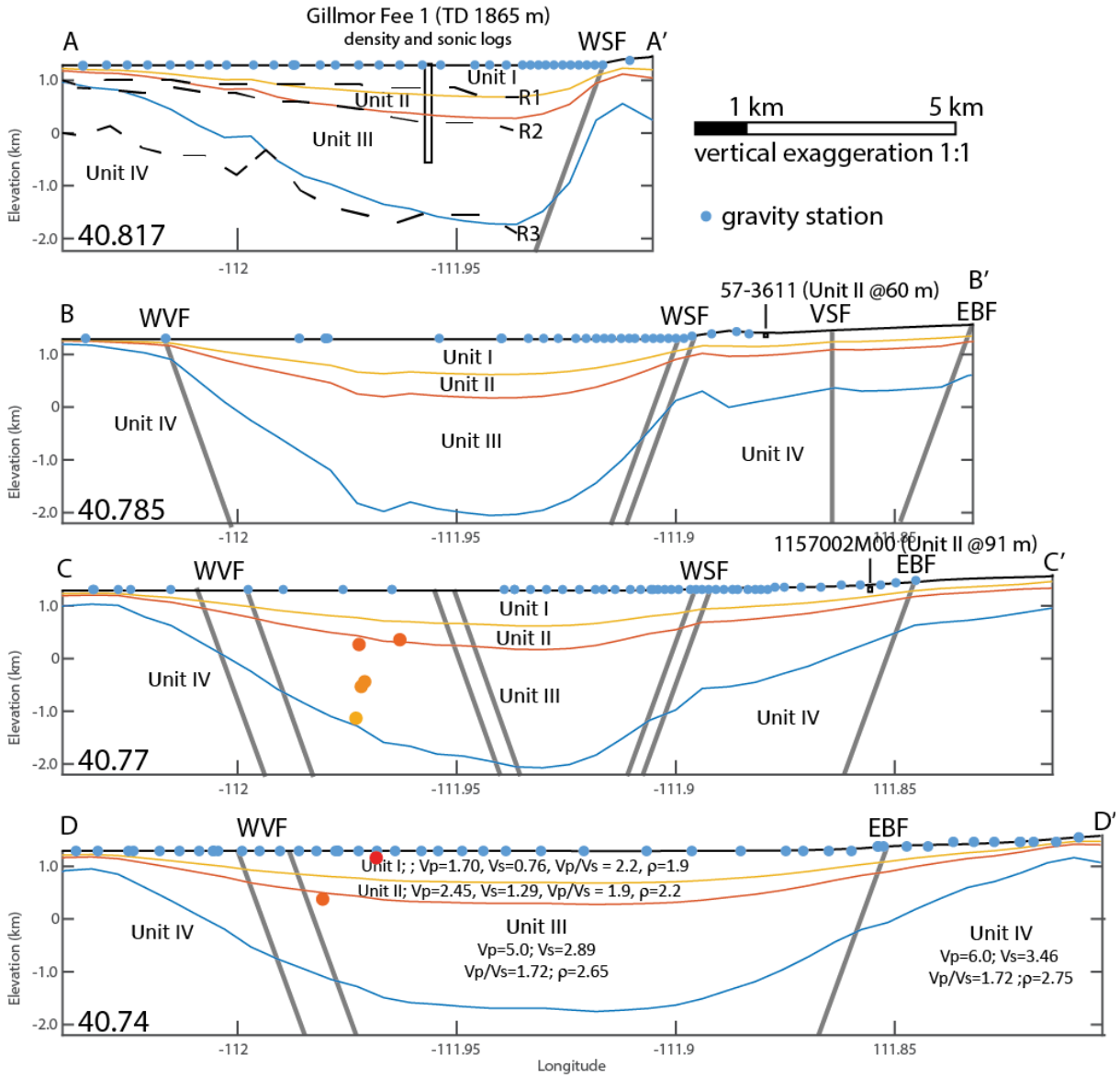

Figure 4. Gravity derived stratigraphic boundaries across the Salt Lake basin. Profiles are shown on Figure 2 and gravity measurements within 200 m of the profile are projected. Profile A-A' shows seismic contacts R1, R2, and R3 (Hill, 1988) and location of the Gillmor Fee 1 borehole that contains density and Vp estimates. A summary of physical properties for each unit appears on profile D-D'. Fault dips are estimated at 70° and surface locations are taken from USGS fault and fold database (http://earthquake.usgs.gov/hazards/qfaults/map/). Earthquakes are projected to profiles.

Figures 2 and 4 shows the results of our gravity analysis where we assume a 0.15 g/cc bulk average difference between Unit IV bedrock and overlying strata (Units I, II and III). With this assumption, we show that the basement geometry along profile A-A' (latitude 40 degrees 49 minutes) is consistent with the R3 boundary mapped with seismic studies (Hill, 1988; Figure 4). The gravity model shows that the maximum basement depth has strong asymmetry along the northern profile where the WSF controls basin subsidence and is symmetric along the southern profiles where late Quaternary mapped faults do not strongly influence basin geometry. The eastern basin margin widens considerably along the southern profiles, consistent with the step over from the WSF to EBF. To estimate the depth to the base of Unit II, we assign a 0.45 g/cc bulk average difference between Paleozoic and older strata and overlying Tertiary and younger strata. This is equivalent to a 2.25 g/cc bulk density for Units I/II and a 2.7 g/cc bulk density for units II/IV (Figure 2). With this assumption of constant density ratios and with comparable depths observed between the base of Unit II and the geometry of reflector R2 along profile A-A' (Figure 3), we estimate the geometry of the Unit II base. Again, this unit is symmetric on all but the northern profile near the WSF. The base of Unit I was estimated by assigning a bulk density difference of 0.75 g/cc between Tertiary and older strata and unconsolidated Quaternary sediments. This density contrast is consistent with a bulk density of 1.9 g/cc over 2.65 g/cc and shows similar geometry when compared to reflector R1 along profile A-A'.

From our analysis, we estimate a 3 km basin depth (-2 km elevation) near the center of the valley, consistent with both Bashore (1982) and Hill et al. (1990) estimates (Figure 4). The Salt Lake basin shallows to the north of our northern transect (A-A'), extends to the south about 15 km, and is about 5-10 km wide with the widest portion of the basin located near transect D-D' to the south of SLC (Figure 2). Near the WSF (profile A-A'), a strong basin asymmetry is observed where the basin (Unit IV) shallows to less than one km depth and the Unit I base shows a change in depth of about 500 m. The abrupt shallowing of bedrock along the eastern portion of profiles A-A' and B-B' is consistent with a 70 degree WSF dip documented by Gilbert (1928) and by Bashore (1982) and suggests that this fault has been active and stationary during basin evolution.

Along profile C-C' (latitude 40 degrees 46 minutes – North Temple Street), an inflection in the bedrock surface (top of Unit IV) at about 1.5 km depth appears along strike of the WSF to the south. This profile is between the Washington School and Salt Palace trenches along North Temple Street. While the bedrock inflection may be related to shallow changes in density or local elevation changes, the change in dips along all unit boundaries is consistent with the WSF extending beneath downtown SLC. Note that the top of Tertiary contours trend N20W between the WSF and EBF south of profile C-C'.

At the latitude of profile D-D' (latitude 40 degrees 44 minutes), the southern projection of the WSF represents the eastern limits of the Salt Lake basin depocenter, but no discrete bedrock step is observed with the gravity model. The shallowing of bedrock to the east may support continued slip along WSF as far south as profile D-D', but decreasing bedrock offset suggests that there is a diminishing influence of the fault near this latitude. Alternatively, the broader anomaly may reflect a distributed zone of faulting with no single bedrock step. In summary, gravity data show the eastward widening of the Salt Lake basin to the south of profile B-B'. Whereas gravity data along the WSF to the north of Salt Lake City is

consistent with a single 70-degree west dipping fault, a zone of distributed faulting and basin downwarping may dominate the eastern basin region beneath, and to the south of, SLC. A change in bedrock geometry along profile C-C' supports the southern extension of the Warm Springs beneath downtown Salt Lake City where overlapping faults related to the Salt Lake segment of the Wasatch fault may coseismically rupture. The top of Tertiary contours between profile C-C' and D-D' trends N20W.

Seismic approach

We acquired approximately 15 km of seismic data over three field days in 2015 and an additional 20 km of seismic data over five field days in 2017 along the heavily trafficked city streets of Salt Lake City (Figures 1 and 3). Data acquisition was conducted during late spring when water table elevations were near median annual levels (e.g., Mower and Van Horn, 1973; Thiros, 2003). The 35 km of new seismic data were collected at a nominal 2 m shot spacing using a 200 kg accelerated weight drop source and a two-component (vertical and in-line), 1.25 m spaced sensors that contained 4.5 Hz baseplate-coupled geophones embedded in fire hose (Liberty and Gribler, 2014). The weight drop source operates directly on city streets during business hours with no resulting road surface damage (Liberty, 2011). A single operator controls the source, recording system, and streamer positioning. The source produces broad band impulsive signals between 3-300 Hz. We pulled our seismic streamer at a distance of 5 m (2015) or 10 m (2017) behind the seismic source. Thus, we collected more than 15,000 48-channel shot gathers with a 60 m receiver aperture. Timing between two meter shots (single hammer hit per location) was approximately 15 s, resulting in about 480 m/hour rate of data acquisition or 4-5 km per day.

We extract vertical component first arrivals to obtain p-wave (Vp) seismic measurements to 20-40 m depth, two-component Rayleigh wave dispersion curves to obtain shear wave (Vs) seismic profiles to 20-30 m depth, and vertical component reflection signals to map subsurface horizons to upwards of 300 meters below land surface. Whereas the maximum depth for refraction and reflection results is strongly tied to the limited geophone aperture, Vs probing depths was additionally limited by source frequencies. We utilize a differential GPS system to obtain decimeter scale position measurements during data collection. We then use Lidar derived elevations (https://gis.utah.gov/data/elevation-and-terrain/2013-2014-lidar/) for subsequent seismic processing. Distances along each profile are with respect to the first source position. Some seismic profiles were obtained with the assistance of a certified road survey crew to control traffic while the downtown profiles were acquired with the assistance of Salt Lake City off-duty police officers.

Late Quaternary seismic properties and character for the Salt Lake basin

For unconsolidated sediments, seismic velocities are strongly controlled by lithology, fluid content and porosity (e.g., Mavko et al., 2009). The largest Vp contrast that we encounter is found at the transition from dry to saturated unconsolidated sediments and at the transition from unconsolidated Quaternary strata to consolidated Tertiary strata. Where saturated unconsolidated sediments are found, we typically observe seismic velocities that exceed the speed of sound in water (about 1,500 m/s). Within the vadose zone, Vp typically ranges from between 350-1400 m/s. Where Tertiary strata are mapped, seismic velocities typically exceed 2,450m/s (Hill et al., 1990). Shear wave velocities are strongly tied to

soil and rock stiffness and less dependent on fluid saturation when compared to p-wave velocities (Boore and Atkinson, 2008; Mavko et al., 2009) In the Salt Lake basin, shear wave velocities in the upper 30 m range from about 150-700 m/s, with the slower velocities typically found beneath the lower elevation regions where late Holocene deposits are mapped (e.g., Personious and Scott, 1992; Williams et al., 1993; McDonald and Ashland, 2008).

A simplified hydrostratigraphy for late Quaternary stage of the Salt Lake basin consists of alternating finer grained lacustrine strata in the lower elevations and coarse-grained near shore deposits and alluvium near the lake margins (Personious and Scott, 1992; Figure 3). The depth to ground water is generally shallow at low elevations, but often under artesian pressure due to fine-grained confining layers (e.g., Mower and Van Horn, 1973; Price, 1985; Thiros, 2003). Perched water above confining units is common, but this zone may be too thin to seismically resolve with our survey. At higher elevations within the Salt Lake basin, the groundwater aquifer is generally deeper and typically unconfined due to the presence of less fine grained materials. Water levels in the wells typically rise by upwards of 3 m during the spring and early summer months and decline the rest of the year (Mower and Van Horn, 1973; Hu et al., 2018). This fluctuation in groundwater elevation is an important component to assessing liquefaction susceptibility in soft sediment low elevation areas (e.g., Olsen et al., 2007) and also can change shallow seismic properties. Artesian springs have been mapped within the footwall of the EBF where the edges of confining beds are exposed and terminate (Mower and Van Horn, 1973) or where the faults act as barriers to lateral groundwater flow (e.g., Caine et al., 1996).

The lacustrine strata at low elevations often produce a high quality seismic reflection character due to the presence of soft, saturated, and laterally continuous Pleistocene strata (sands, silts and clays) where saturation drives Vp typically above 1,500 m/s and loose soils drive Vs to very low values. Where complex near surface structures are present (e.g., lateral spread deposits), the underlying reflection character can degrade due to scattering and attenuation. Along the basin margins, the coarse grained materials within shallow alluvial deposits often lack a uniform internal architecture, are stiffer (higher Vs) than the lacustrine deposits, and the water table is deeper (lower Vp) when compared to lower basin elevations. Thus, low elevation areas beneath SLC typically contain high Vp/Vs ratios and high elevation areas typically contain low Vp/Vs ratios. Within many active fault systems, soil properties within a fault zone can lead to faults acting as conduits or barriers to groundwater flow (e.g., Caine et al., 1996). Vp/Vs ratios can provide fluid and matrix values within the faults to further constrain fault properties.

Vp derived from head waves

We identify the first arrival time as the first ground motion for each source/receiver pair (Figure 5). First arrivals were picked both from unprocessed field records and filtered field records in both shot and offset domains. Given the large seismic energy source with respect to limited receiver offsets, first arrivals on an asphalt road surface were typically clean and easy to pick in the presence of traffic noise (Figure 5). We were unable to utilize refraction picks on concrete roads where arrivals from the road surface appeared as the first ground motion. Where large voids (e.g., storm drains) were located

beneath the road surface, first arrival patterns were more complex and were selectively analyzed. Vp values in about the upper three meters are poorly constrained due restricted geophone offsets.

We use a travel-time tomography code to estimate the shallow velocity structure (modified from St. Clair, 2015). The velocity model is parameterized as a mesh of constant velocity cells with a fixed horizontal width and a vertical thickness that increases with depth. The strategy is to generate a reasonable starting model and then alternate between: 1) shortest path ray-tracing (Moser, 1991) to predict travel-times for the current model and 2) using a linearized inversion with smoothness constraints to map the residual travel-times (predicted – observed) into an updated model with a smaller root mean squared (RMS) misfit (e.g., Zelt et al., 2013). The process is terminated when RMS misfit between successive iterations becomes negligible.

Quantifying model uncertainty and resolution of tomographic models is a difficult task because of the large number of models that need to be tested. Uncertainty tests that explore the relationship between starting models and final solutions can show standard deviations upwards of 25% for individual model parameters. Higher values (>15-20%) typically correspond to regions with strong velocity gradients or low ray coverage, but similar results are observed when comparing results from different algorithms (Zelt et al., 2013). Even in the presence of these uncertainties, large scale features such as depth to bedrock and strong lateral velocity changes tend to be well resolved using any refraction analysis approach.

Vs derived from Rayleigh waves

The Rayleigh wave signals were extracted and processed via the multichannel analysis of surface wave (MASW) approach (Park et al., 1999) using both Kansas Geological Survey Surfseis software (http://www.kgs.ku.edu/software/surfseis/) and in-house Matlab code for picking two-component data (Gribler et al., 2016). The Rayleigh wave signals provide estimates of subsurface elastic (stiffness) conditions where rapid data collection is possible without compromising results when compared directly measuring shear wave velocities through head wave or downhole measurements (e.g., Stephenson et al., 2005).

Frequency-phase velocity dispersion plots were generated for each (2 m spaced) shot gather and peak semblance picks from these plots were inverted to generate Vs profiles for the upper 25-30 m (Figure 5). Rayleigh wave frequencies that are recorded with the land streamer system typically range from 3-60 Hz (e.g., Gribler et al., 2016). Once Vs profiles were calculated, 1-D velocities were combined to obtain 2-D Vs profiles with depth. Vs30 values were then calculated for each receiver spread midpoint location (e.g., Boore et al. 1993), averaging and smoothing values over the 60 m streamer length. We integrate all new measurements with existing regional point measurements compiled by McDonald and Ashland (2008) to map shallow soil classes and compare these class values to mapped geology, elevation and basin geometry; to produce a Vs30 map for the downtown Salt Lake City region to estimate site response during earthquake ground shaking; and to identify lateral spread deposits and assess liquefaction susceptibility.

We adopt the NEHRP soil classification to describe Vs (IBCO, 2000). Here, we describe E-class (less than 180 m/s) as soft soil; D-class between 180-360 m/s as stiff soil; C-class between 360-760 m/s as dense soil or soft rock; and B-class above 760 m/s as rock, locally correlated with Tertiary strata. For display, we use NEHRP sub-classifications of Wills et al (2000).

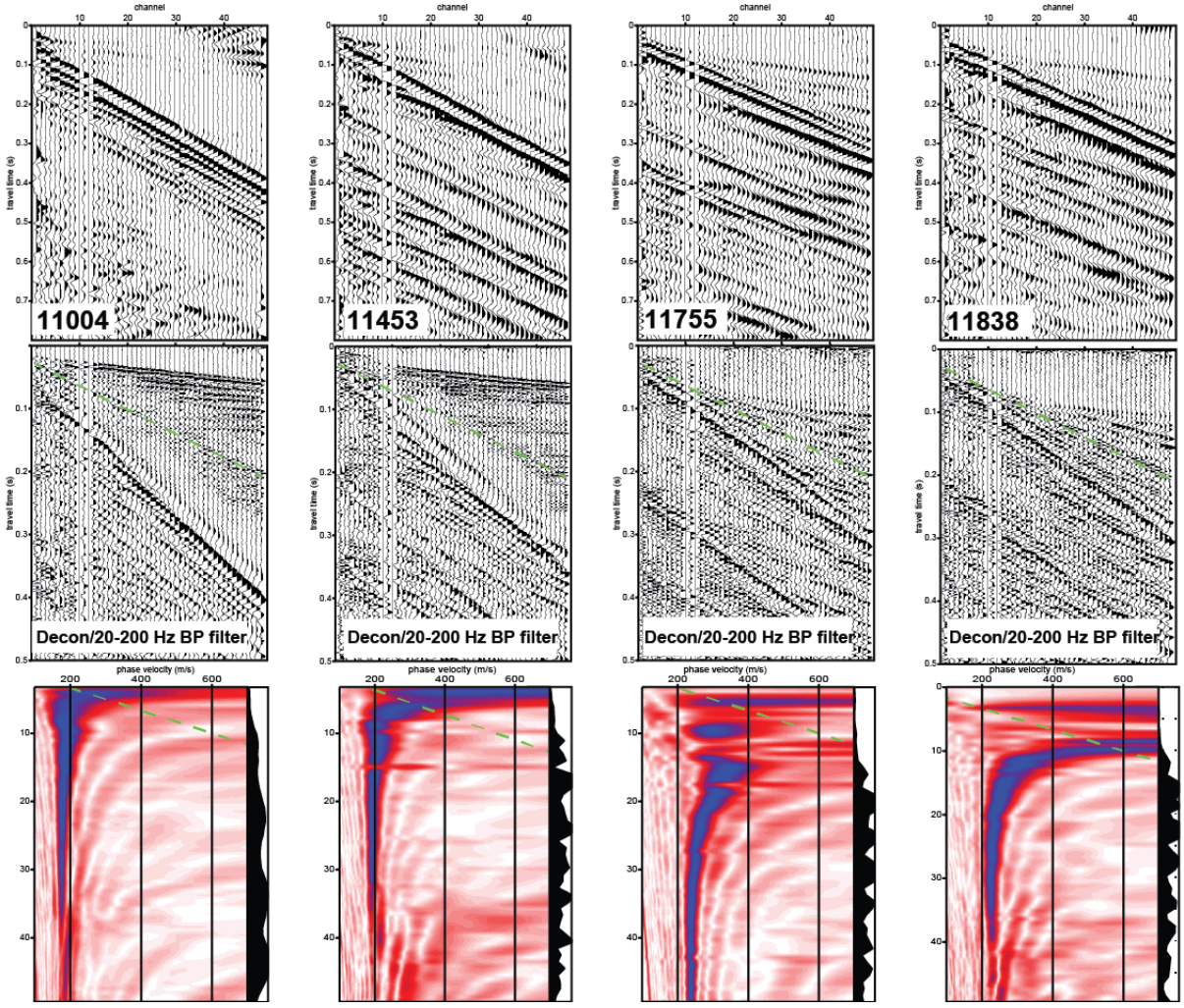

Figure 5. Unprocessed gathers, deconvolved and filtered gathers, and dispersion plots for four shots along 400 East. Green dashed line in middle plot represents the speed of sound in air, and on the bottom plot represents aliasing limits of the data.

Reflection profiling

With the use of 4.5 Hz geophones that optimize the recording of low frequency surface wave energy (to image Vs to greater depths), reflection signals at high frequencies (above 100 Hz) at near offsets were compromised (Figure 5). For single element geophone recording, surface waves tend to dominate the recording systems dynamic range at near offsets and little usable reflection signal is often observed within the surface wave window (even with aggressive surface wave attenuation approaches). To confidently identify seismic reflections in near surface data, we look at coherent arrivals between first

arrival head waves and Rayleigh wave signals with stacking velocities consistent with Vp derived from our refraction analysis. This reflection window has been termed the “optimum window” (Hunter et al., 1984) and for shallow, limited aperture seismic surveys where single element low frequency (4.5 Hz) geophones are used, this window contains reflection signals that are not contaminated with surface waves. The optimum window narrows where higher mode surface waves from complex near surface conditions, are present. Where high Vp/Vs ratios are found, we have a large optimum window (Figure 5a/b) and where low Vp/Vs ratios are found, reflections are more difficult to isolate from head wave and surface wave signals (Figure 5c/d). Thus, the optimum window is reduced in the higher elevation regions of the basin where dry stiff alluvium dominates the near surface.

We processed the data using Halliburton’s ProMAX® seismic processing software with a standard processing approach outlined by Yilmaz (2001). Geometry was applied to each source and receiver location from differentially corrected GPS positions recorded each shot record and via LIDAR-derived elevation values. Processing steps included datum statics, spiking deconvolution, bandpass filter, surface wave attenuation through a two-step singular value decomposition approach to estimate and adaptively subtract the ground roll signal, iterative velocity analyses with dip moveout corrections, amplitude gains, and a post-stack time to depth corrections. Post-stack migration is selectively applied to the data, but migration artifacts can distort key reflector geometries and are used selectively. Where surface waves dominate the gathers and signal processing steps, bottom mutes were applied to remove this signal and improve stacked reflection results. Depths were estimated using a smoothed stacking velocity and refraction model. Where large variations in surface topography is present, we display our gathers in travel time. Water well and engineering borehole logs help constrain lithology and depth to water table for interpretation.

Seismic Results

We first present our seismic results from west to east profiles, from north to south. The northern profiles extend across known strands of the WSF beneath north SLC. Next, we present results of profiling through the downtown corridor where the WSF is inferred, but not directly mapped. We then present results from two 5 km long seismic profiles that are located to the south of any inferred fault strands related to the WSF. Our three 5 km long profiles extend across the EBF to provide continuous profiling across SLC. We also present results from south to north profiles that tie our west-east profiles and cross structures parallel to the EBF and west-trending Virginia Street fault. There is no known Quaternary motion along this fault, but separates Quaternary strata in the basin from Tertiary strata in the Wasatch Range (Figure 3; Personious and Scott, 1992).

The Warm Springs fault beneath North Salt Lake City

The WSF forms a prominent escarpment along the eastern flank of the Salt Lake salient, then is mapped as subparallel fault strands to the south of where the topographic scarp diminishes (Figure 1). Robison and Burr (1991) identified six to eight latest Quaternary events with displacements totaling 14-16 m at the Washington School site (Figure 3). Gravity models suggest about 3 km of basement offset along a ~70 degree west dipping fault and about 0.5 km offset of post-Neogene strata (Figure 4a). Tertiary strata

are mapped immediately north of our survey area (Figure 1) and are identified at about one km depth in the Salt Lake basin center (Hill et al., 1990; Figure 4). We present seismic transects acquired in 2015 along the mapped portion of the WSF to document the location of the WSF. We then show the 2017 profile along North Temple. We show lateral reflector and velocity discontinuities that highlight soil and fluid properties, and relationships to changing topography. We present our reflection results as unmigrated, travel time images due to marginal signal quality and steep surface slopes. This low quality reflection result is, in part, due to alluvial fan surface deposits and laterally changing strata at the margin of the Salt Lake basin. As a result, we will discuss only reflector truncations and character.

Our 460 m long west-east West Girard profile extends across the eastern strand of the WSF (Figures 1 and 3). The profile climbs a topographic slope that gains 40 m in elevation from west to east with a topographic inflection about 100 m from the end of profile (Figure 6). Holocene to Upper Pleistocene undifferentiated alluvial fan deposits are mapped along the profile and Tertiary rock exposures are mapped immediately north of the eastern portion of the profile (Personious and Scott, 1992). The eastern strand of the WSF is mapped near the center of the profile. Refraction and reflection results are consistent with a down to the west normal fault at the westward termination of the 2,450 m/s Vp contour. Lateral termination of this top of Tertiary marker is consistent with the inflection in topographic slope. This eastern strand of the WSF (McKean, 2014) separates reflections of differing dip, but it is unclear from this profile the amount of slip across this fault due to the lack of reflector continuity across the fault. An arcuate reflection in the hanging wall side of the fault is consistent with a drag fold.

The 500 m long 500 North Street profile lies upon Holocene to Upper Pleistocene undifferentiated alluvial fan deposits (Figure 3). The western strand of the WSF is mapped along the western portion of the profile. A fault identified in the Washington Elementary school trench, immediately south of 500 North, is interpreted as a step over between two north-south fault segments (McKean, 2014). A high amplitude reflector at about 10-40 m depth below land surface, along with a jump in refraction velocities to above 1,500 m/s, is consistent with the transition from dry to saturated sediments (Figure 6). This interpretation is supported by the nearby water well 57-8417 that shows a 35 m depth water table (http://www.waterrights.utah.gov/wellinfo/wellsearch.asp). The water table abruptly steepens at position 300 m, possibly related to a fault. Reflections that lie below the water table reflector dip into the fault, again consistent with a drag fold within the hanging wall along a strand of the WSF.

The Zane Street profile is the eastern continuation of the 500 North profile and is located approximately 85 m to the south of the Girard profile (Figure 3). A lateral truncation in Vp > 1,000 m/s at about 20 m depth support the southern extension of the eastern strand of the WSF to this latitude (Figure 6). At this same location, an offset reflector is consistent with down to the west motion.

The 400 North/Apricot transect is comprised of three profile segments (Figure 3). The flat lying portion of 400 North lies upon younger Holocene to Upper Pleistocene undifferentiated alluvial fan deposits (Figure 3; Personious and Scott, 1992). The middle segment of this transect transitions from fan alluvium to upper Pleistocene lake deposits. A slope break appears along the eastern portions of this segment.

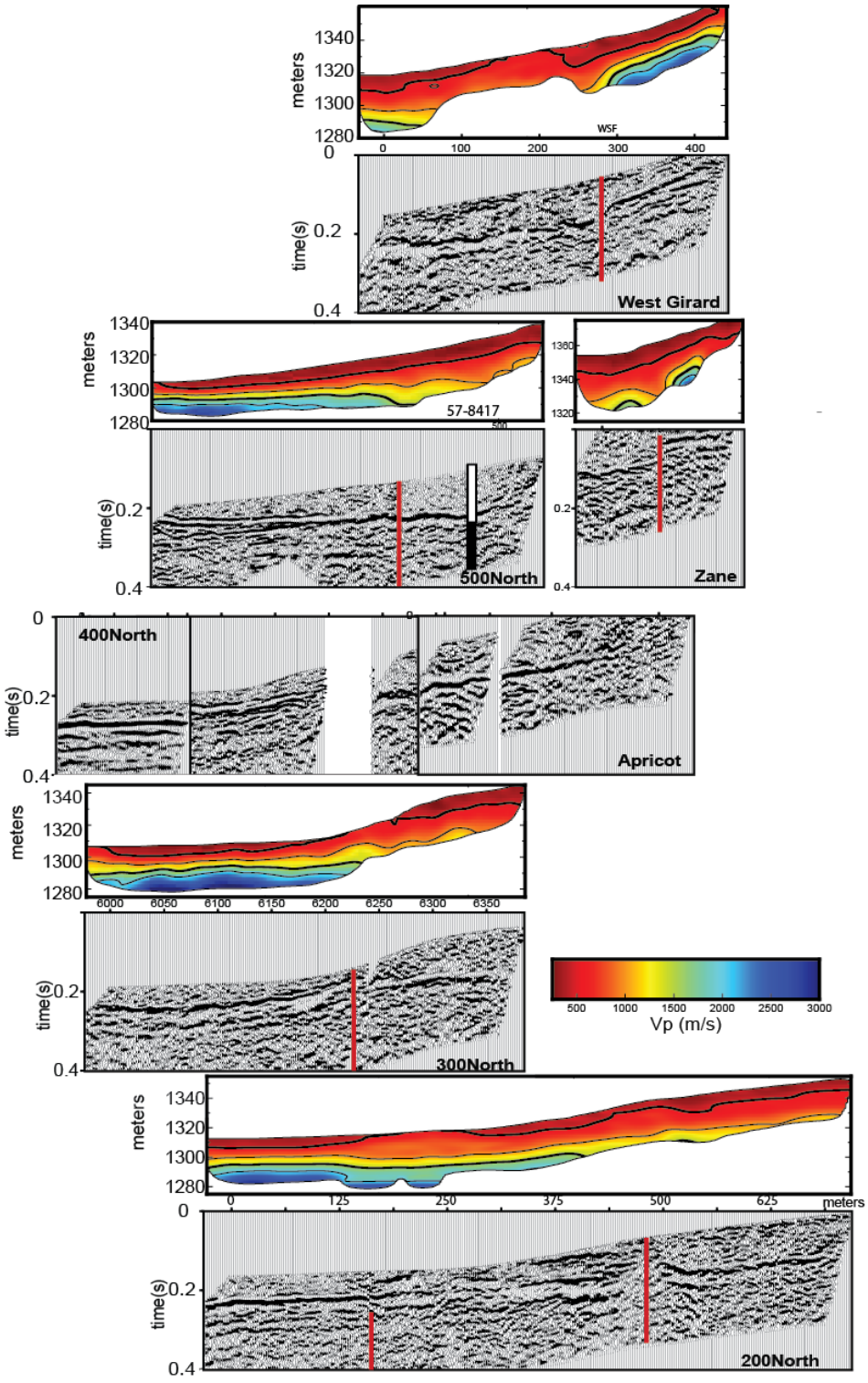

Figure 6. Vp and reflection results for profiles in North SLC acquired in 2015, aligned by longitude. Figure 3 shows detailed locations. Strands of the Warm Springs fault appear as lateral truncations of reflection and Vp.

East of 400 North, the transect continues along Apricot Street east to within one block of the state capitol building where Upper Pleistocene lacustrine sand and gravel deposits are mapped. McKean (2014) mapped the western strand of the WSF along the eastern edge of the 400 North profile and the eastern strand beneath the central Apricot Street segment. Seismic imaging shows a strong amplitude reflector and large seismic velocity increase at about 10-30 m depth, consistent with the water table depth from nearby water wells. This reflector roughly follows topography, but deepens from west to east. Due to the short segments along this transect, we do not include Vp profiles, but a decrease in seismic velocity, a break in the topographic slope, and a disrupted water table reflector along the eastern portion of the 400 North profile points to a strand of the WSF system mapped by McKean (2014). We interpret a second strand of the WSF at a second slope break beneath Apricot Street. A step in reflector depths and continuity between 400 North (center) and Apricot Street profiles may point to an additional fault strand. At the eastern fault location, reflectors beneath the water table are discontinuous. Although bedrock likely shallows to the east along this profile, refraction and reflection data do not constrain the bedrock depth.

The 525 m long 300 North profile lies upon Holocene to Upper Pleistocene undifferentiated alluvial-fan deposits along the western portions of this profile (Personious and Scott, 1992) with Upper Pleistocene lacustrine sand and gravel along the eastern reaches of the profile (Figure 3). McKean (2014) mapped only the western strand of the WSF beneath this profile, with the eastern strand terminating immediately to the north. A step in both Vp and Vs approximately 100 m to the east of the profile start suggest a change in lithology and is consistent in location with a strand of the WSF. Dipping reflectors beneath the water table also support the interpretation. We map a second fault strand at the change in topographic slope near the center of the profile. At this location, slower p-wave and s-wave velocities are mapped to the east and there is a change in reflection character to denote the eastern strand of the WSF.

The 200 North profile is located between 200 West and North State Street (Figure 3). Elevation increases along the length of the profile from west to east, with an inflection in topographic slope near West Temple Street (Figures 3 and 6). The WSF is mapped between 200 W and West Temple near the western limits of the profile and Holocene to Upper Pleistocene undifferentiated alluvial-fan deposits are mapped beneath the profile (Personious and Scott, 1992). We map three strands of the WSF along this profile. The western strand is based on reflector truncations below the water table and an increase in Vp and Vs. The center and eastern fault strand is based on an inflection of the surface topography, water table and deeper reflections and lateral changes in Vp and Vs.

In 2017, we acquired the North Temple seismic profile (Figures 1 and 3) where we extended our near source to receiver offset from 5 m to 10 m to imaging capabilities at depth. This profile was heavily trafficked during acquisition and storm drains were mapped below the road surface, thus reducing signal quality (most notably on the Vp profile where first arrivals were difficult to confidently pick at long offsets). The profile lies upon Holocene fan alluvium (Personious and Scott, 1992) and the land surface increases in elevation by about 50 m (Figure 7). The most notable feature on the seismic refraction image is a step in Vp near position 800 m. This velocity step is noticeable to as shallow as 10 m depth

along the 1,000 m/s contour, above the water table. At this location, a Vs inversion with depth is noted, where NEHRP C-class soils lie above D-class soils. This Vs velocity inversion is consistent with lateral spread deposits that are observed on many of our downtown seismic profiles (but not currently along this profile). The depth to water table is more than 20 m at this location, suggesting that the risk of liquefaction from lateral spreading during future earthquakes may be lower than other areas of SLC.

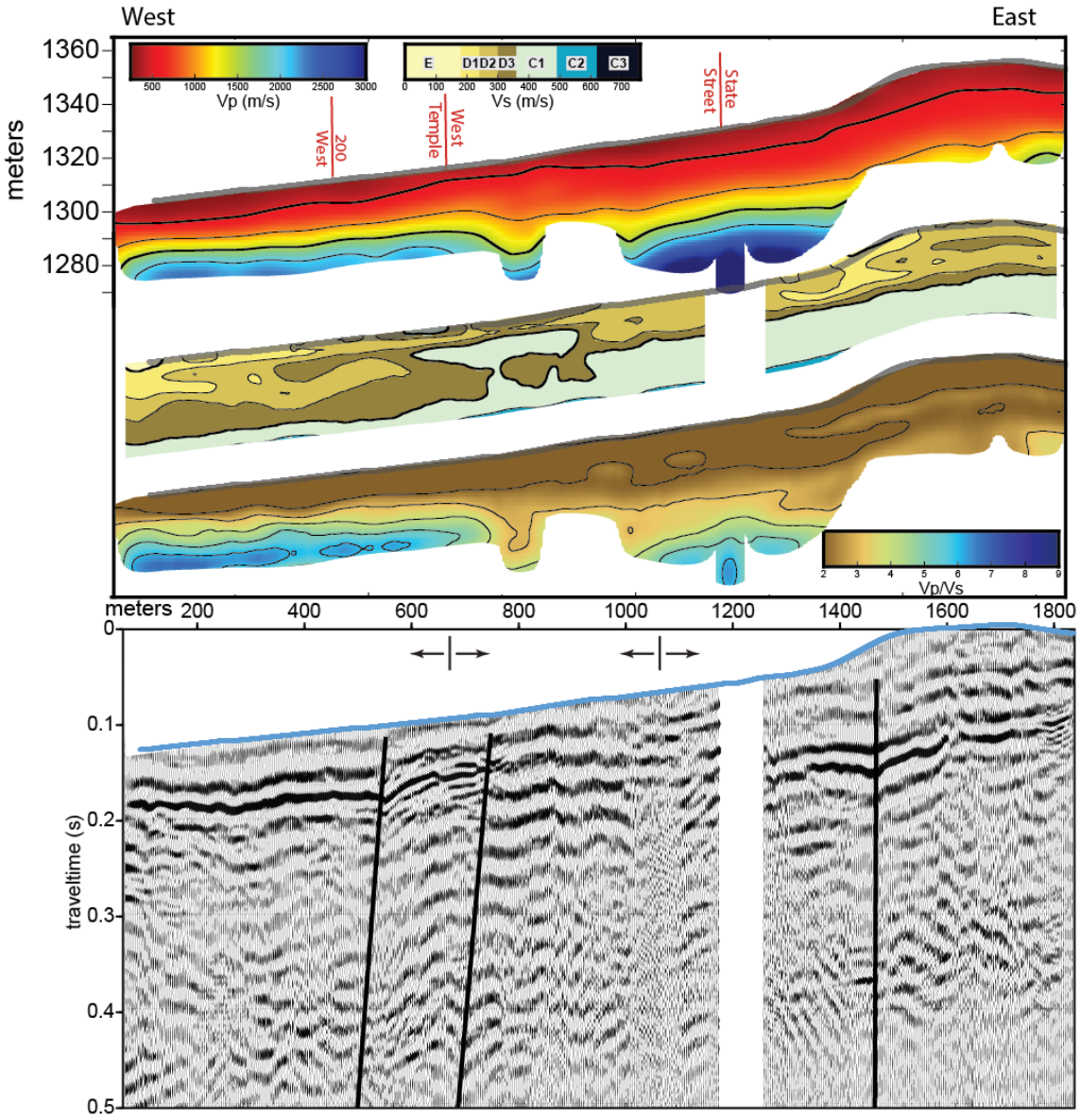

Figure 7. Vp, Vs, Vp/Vs, and reflection results for the North Temple profile (see Figure 3 for location). Note the step down in Vp contours and Vs velocity inversion near position 700-800 m. NEHRP Class C1 (dense) soils from 3-10 m depth may represent lateral spread deposits. The reflection results show reflector truncations and folding that are consistent with faults.

On the reflection profile, we note a lateral truncation in reflections at the location of the Vs velocity inversion and the step in Vp between 700-800 m (Figure 7). To the west, folded strata are consistent with faults that bound the zone of liquefaction. We interpret this boundary to represent the southern extension of the WSF (Figure 3). This fault location lies between the Washington School trench and the Salt Palace, consistent with the fault interpretation of McKean (2014). Near position 1450, an inflection in Vp contours matches the location of changing reflector geometries where we interpret a fault where strata to the west are folded into a fault. We interpret this fault as the southern extension of the eastern strand of the WSF that is mapped along Girard, Apricot and 200 North profiles (Figure 3).

200 South profile

The 2015 4.5 km long 200 South profile extends from 500 West to the University of Utah campus (Figure 1 and 3). The profile begins upon Holocene lacustrine deposits and transitions to fan alluvium near position 500 m. Fan alluvium and late Pleistocene lacustrine deposits are mapped to the eastern limits of the profile (Personious and Scott, 1992). Southward projection of the WSF near the Salt Palace is between positions 900-1350 m and the EBF is mapped near position 3600 m. Cultural noise along this line was strong, especially due to light rail lines that run along the street.

Vp results show low velocity (<500 m/s) in the upper 10 m beneath a topographic bulge between positions 500-1800 m (Figure 8). We interpret these low velocities to represent Holocene fan alluvium that has been deposited after the final Bonneville transgression. These low velocities are also found between 220-4500 m distance, consistent with mapped fan alluvium of Personious and Scott (1992). We note a prominent step down to the east in the 1,500 m/s contour at position 2200 m and steps down to the west at positions 3550 m and 4150 m. These lateral truncations are consistent with an abrupt change in water table elevation. The 1,500 m/s Vp contour is highly variable along this profile, consistent with lateral changes in lithology and fluid properties.

NEHRP Class E soils, derived from Vs, are mapped in the upper 10 m to the west of position 500 m (Figure 8), consistent with Holocene lacustrine deposits mapped by Personious and Scott (1992) (Figure 3). A sharp increase in Vs between 1,000-1,500 m is consistent with lateral spread deposits mapped near the Salt Palace (Figure 3; Personious and Scott, 1992). These higher velocities are best noted with the Vs30 profile where bulk Vs increases by about 30% when compared to areas to the west and east. NEHRP C-class dense soils are mapped below 15 m depth to the east of 2,000 m, consistent with older (late Pleistocene) lake deposits. An inflection in Vs is noted near position 4,200 m, consistent with a change in depositional or structural dip.

Vp/Vs ratios highlight changes in fluid saturation across 200 South (Figure 8). We note a very shallow water table to the west of 500 m (Vp/Vs >7). Lower Vp/Vs ratios are found beneath the Salt Palace (between 200 West and West Temple). Low Vp/Vs values are noted at positions 2200 m, 3500 m, and 4150 m, consistent with dry, stiff soils within a narrow zone.

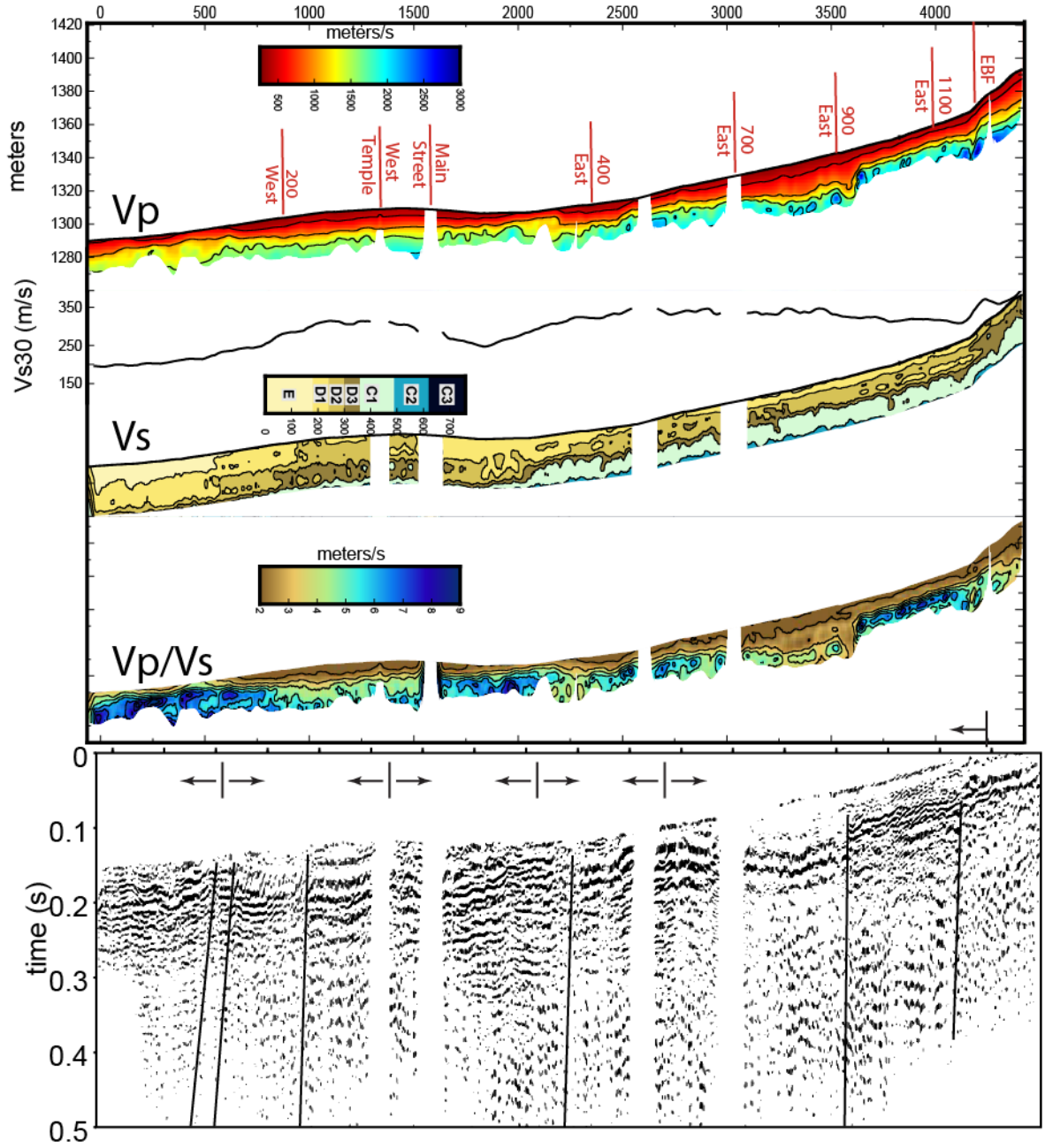

Figure 8. Vp, Vs, Vs30, Vp/Vs, and reflection results for the 4.5 km long 200 South profile (see Figure 3 for location). Complex Vp and Vs distributions in the upper 30 m lead to poor reflection imaging at greater depths. However, folding and faulting is noted across the profile.

In addition to cultural noise of downtown SLC, the seismic reflection profile is very noisy due to complexities in the near surface that include the presence of high amplitude higher order surface waves (overtones) and laterally changing Vp and Vs values. These complexities lead to wavefield scattering and contamination of surface waves into the body wave "optimum window". However, in the presence of the noise, we observe multiple reflector truncations and folds in the shallow strata.

At positions 600 m, 1250 m, 2000 m, 2700 m, and 4200 m, we identify the crest of folds. Between these folds, reflector truncations are consistent with faults. In particular, mapped faults beneath the Salt Palace (near 200 West) and farther east correlate with lateral truncations in Vp and Vs. This suggests that these faults offset strata in the upper 10 m, or latest Pleistocene Bonneville strata. The tie between low Vp/Vs and the presence of faults suggests that the faults are barriers to lateral groundwater flow with a grain size redistribution within the fault zone.

400 South CPT survey

Leeflang (2008) acquired eight CPT soundings along 400 South and an additional two soundings along 500 South (Figure 3). Along 400 South, they identified west-dipping Lake Bonneville strata to the west of State Street (Figure 9). Between State Street and 300 East, they identified the crest of a broad fold. Between soundings CP-4 and CP-5, they identified 8.7 m vertical offset at the base of Bonneville strata and between soundings CP-5 and CP-6, they identified an additional 3 m offset. Although topography along the stratigraphic surface may vary across the survey, these measureable offsets are consistent with down to the west faulting associated with the along strike extension of the WSF (near CP-4).

Correlation of Stratigraphic Units along 400 South Street — from Leeflang (2008)

Unit	Age/Description	Symbol (Leeflang, 2008)	Mapped Geology (Personious and Scott, 1992)	density
Upper Bonneville Formation – Unit 3	Upper Pleistocene/clays and silts associated with final transgression of Lake Bonneville	UBF3	Qlbpm	1.8
Upper Bonneville Formation – Unit 2	Upper Pleistocene/thinly bedded highly variable deposits associated with regression of Lake Bonneville following its high-stand	UBF2	Qlbpm	1.9
Upper Bonneville Formation – Unit 1	Upper Pleistocene/thinly bedded clay/silt/minor fine sand associated with regression of Lake Bonneville following its high-stand	UBF1	Qlbpm	1.9
Lower Bonneville Formation – Unit 2	Upper Pleistocene/clays and silts associated with deeper water deposits of Lake Bonneville	LBF2	Qlbpm	1.8
Lower Bonneville Formation – Unit 1	Upper Pleistocene/clays and silts associated with deeper water deposits of Lake Bonneville	LBF1	Qlbpm	1.3
Pre-Bonneville – Unit 1	Middle Pleistocene/alluvial gravels with interbedded silt	APF2	Afo	2.1
Pre-Bonneville 2 – Unit 2	Middle Pleistocene/interbedded alluvial silt and clayey silt	APF1	Afo	1.9

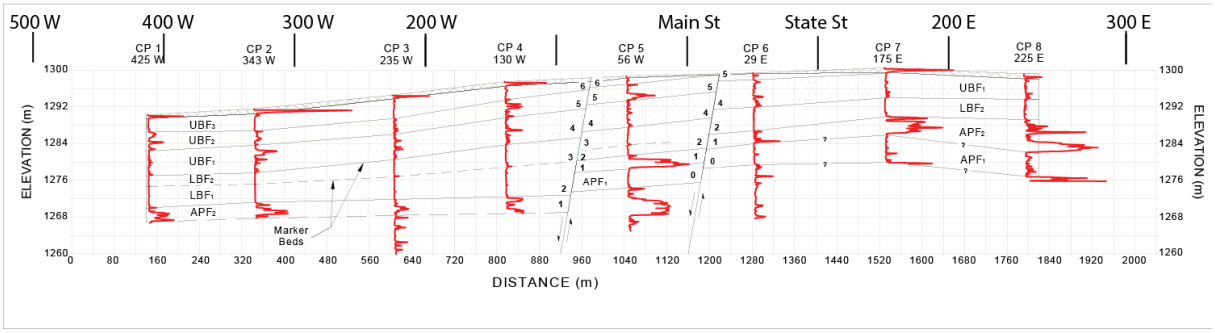

Figure 9. CPT results from Leeflang (2008). The table shows lithologies interpreted from tip resistance results. Densities are estimated in g/cc (bottom) Tip resistance CPT soundings. Higher tip stress values indicate relatively stiff sediments (e.g., gravels, sands or non-plastic silts); lower tip stress values indicate plastic silts and clays. This report suggests 8.7 m of vertical offset in 20-30 ka Lake Bonneville strata between CP-4 and CP-5 and 3 m of vertical offset between CP5 and CP-6.

500 South seismic profile

The east to west 1.35 km 500 South profile was acquired in 2017 and extends from State Street to 700 East and crosses profile 400 East at position 750 m (Figures 1 and 3). The profile sits upon Bonneville lake deposits with lateral spread deposits mapped between positions 300-700 m (Personious and Scott, 1992). The lateral spread was mapped from excavations at the Hall of Justice (Figure 1) that revealed numerous high-angle faults and other deformation features (Scott and Shroba, 1985), but there was no clear evidence that lateral spread was rooted in deep seated faults. The elevation rises from 1297 m to 1312 m, between Gilbert and Provo high stands, and the source to near geophone offset was 10 m for this profile.

Vp ranges from about 600 m/s at the land surface to about 2,200 m/s at about 20 m depth, consistent with lake Bonneville unsaturated and saturated sediments (Figure 10). The 1,500 m/s contour ranges from 8-15 m depth, is consistent with water table elevation recorded in nearby wells (http://www.waterrights.utah.gov/wellinfo/wellsearch.asp), and parallels the land surface along much of the profile. Vs for the upper 20 m is mapped as NEHRP D1 class (180-240 m/s) class stiff soils, except for between positions 700-1000 m where mostly NEHRP D2 class soils are recorded over 1-3 m of NEHRP E-class soils. We note a Vs velocity inversion (slower phase velocities at lower frequencies) within this zone, consistent with sediment repacking from lateral spreading (e.g., Obermeier, 1996) overlying undeformed lacustrine strata. Near the western portion of the profile, Leeflang (2008) acquired two CPT soundings that show large lateral changes in lithology and physical properties over a distance of about 100 m. They concluded sediments of relatively different ages and origins have been juxtaposed between the two adjacent soundings. Figure 11 shows tip resistance measurements for the CP-9 and CP-10 surveys where high tip resistance related to faster (more stiff) Vs values. The CPT measurements support the Vs velocity inversions with depth, attributed to the zone of high Vs that corresponds with mapped lateral spread deposits (Personious and Scott, 1992; Figure 1).

On Figure 10, we show a common offset gather from 500 South (panel D). This single channel profile highlights the effect of lateral spread on the seismic data. The largest amplitude signal from our land streamer survey is derived from Rayleigh waves (between 0.2-0.4 s time) that propagate between 5-50 Hz. At the location of the mapped lateral spread deposits at the Hall of Justice site (Scott and Shroba, 1985; Qml on Figure 10), we measure a noticeable travel time difference for the largest amplitude signal. For this 65 m offset gather, we show an increase from about 200 m/s along most of the profile to about 280 m/s for a 200 m length surrounding mapped lateral spread deposits. From liquefaction, a rearrangement of grains into a denser packing structure decreases porosity by increasing soil density (e.g., Obermeier, 1996); thus an increase in soil stiffness or increased Vs compared to in situ strata. Here, we show a 40% increase in Rayleigh wave speeds related to paleo-liquefaction within Upper Bonneville deposits.

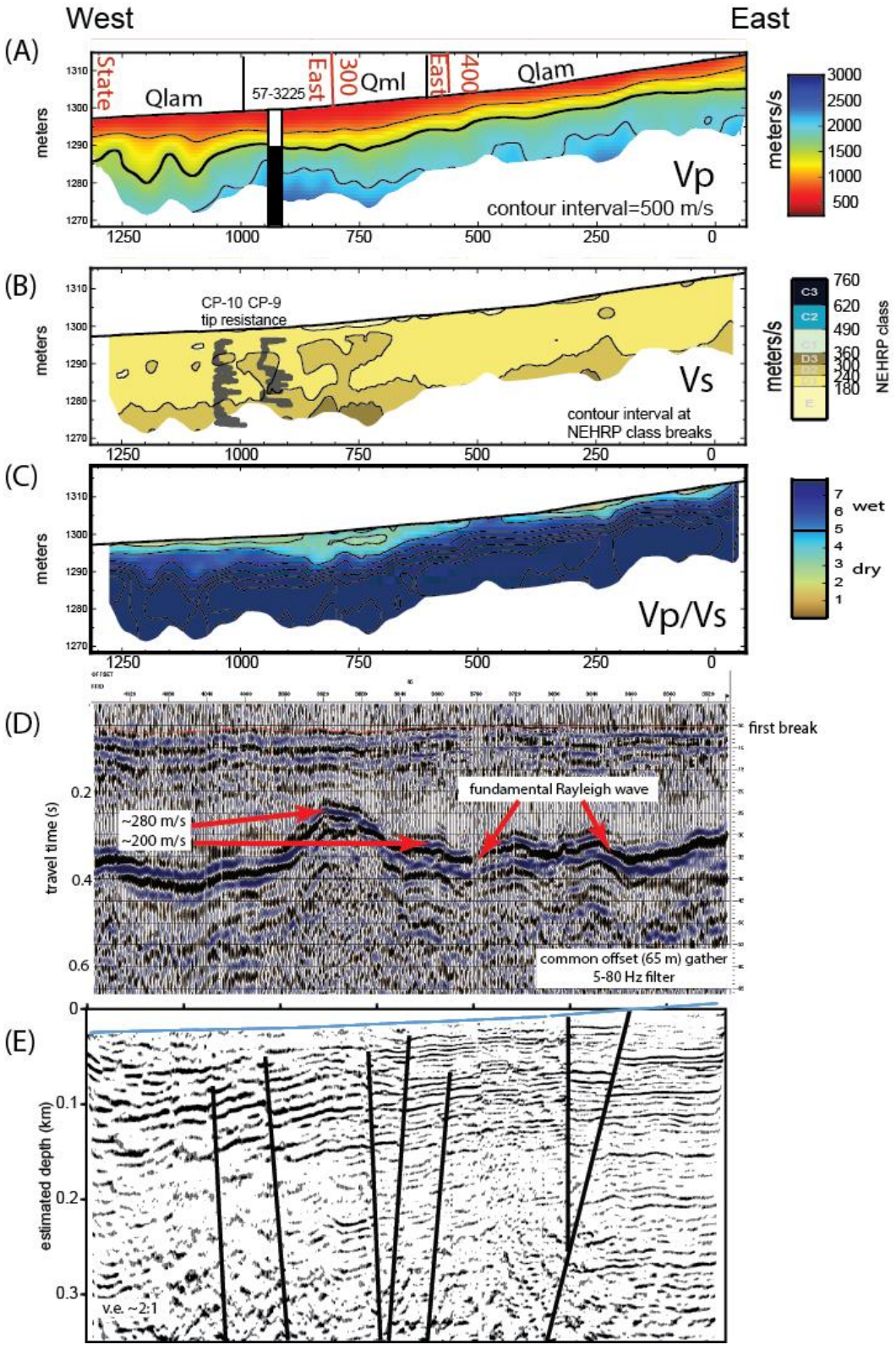

Figure 10. Vp, Vs, Vs30, Vp/Vs, common offset gather, and reflection results for 500 South.

The reflection image shows high quality, gently west dipping reflectors along the western one km of the profile and flat lying strata along the eastern portion of the profile (Figure 10). We observe continuous reflectivity to about 300 m depth. Because our gravity model suggests greater than a 500 m depth to Tertiary rock, we interpret these dips as part of the west limb of a gentle fold that lies within late Quaternary strata. This is consistent with the CPT survey one block to the north (Leeflang, 2008), with the crest of the fold approximately 500 m to the east along 500 South. From offset reflectors that increase in offset with depth, we interpret a zone of growth faulting beneath much of the western and central portions of the profile. We conclude that the 200 m wide zone of lateral spread deposits deform Late stage Bonneville deposits and are rooted in active faults related to the WFZ.

700 South/800 South

We use the 700 South (acquired in 2015) and 800 South profiles (acquired in 2017) to characterize the late Quaternary basin evolution in the step over region between faults. These two profiles, spaced one block apart, extend across the eastern half of the Salt Lake basin, across the southern projection of the WSF, and across mapped strands of the EBF. No prior evidence for faulting or liquefaction is documented to the west of the EBF at this latitude (Figure 1). The 5 km long 700 South profile extends from 600 West to the Mount Olivet cemetery near 1400 East (Figure 3). The 4.8 km long 800 South profile, located about 235 m to the south of the 700 South profile, extends from 600 West to 1400 East.

Personious and Scott (1992) mapped progressively older strata from west to east along these profiles. Modern flood plain deposits related to the Jordan River were mapped below an elevation of 1290 m at this latitude. Along 700 South, these deposits are found west of position 400 m (near cross street 350 West) and along 800 South, over bank deposits are found west of position 700 m (near cross street 400 West). West of position 3500 m on both profiles, the Lidar-derived surface topography slopes about 1.5-2 degrees. To the east of the mapped stream deposits, an eastward progression from Holocene to latest Pleistocene lacustrine, marsh and alluvial deposits are mapped (Figure 11). A slight increase in slope near 2000 m along 800 South is coincident with the Gilbert high stand between 1295-1297 m elevation. Between position 3500 m and the mapped EBF location, surface slopes gradually increase to 8-10 degrees. A 200 m wide zone of colluvium and fan alluvium is mapped above a wider zone of late Pleistocene lake deposits within the fault zone. The land surface above the footwall wall of the fault slopes about 3 degrees to the west, then increases again to between 4-6 degrees near the eastern termination of the profile.

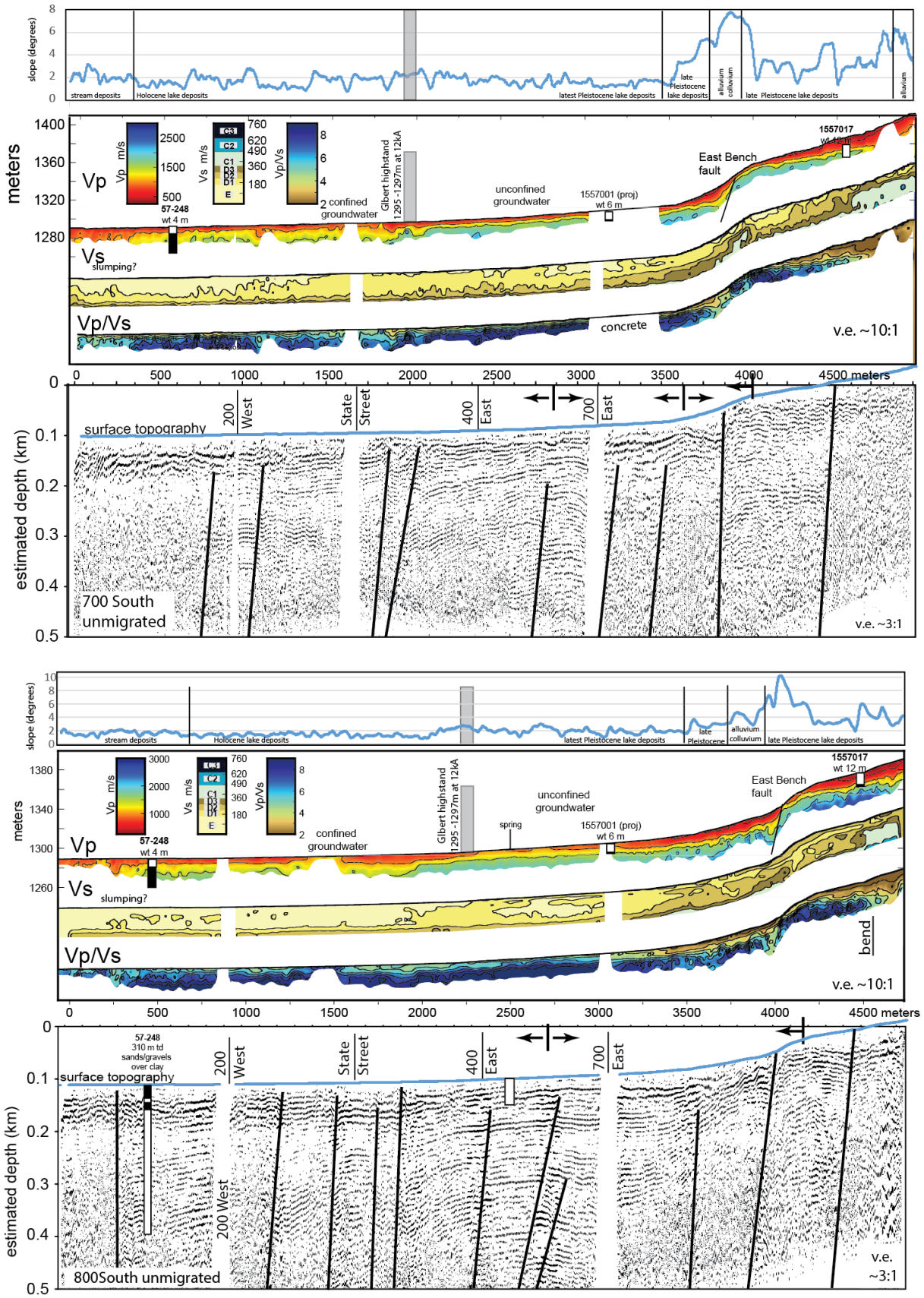

Figure 11. Topographic slope, Vp, Vs, Vp/Vs and reflection results for 700 South and 800 South.

We measure low Vp and Vs to the west of position 1500 m along 700 South and west of position 2000 m along 800 South (Figure 11). To the west of the latest (Gilbert) high stand at 1295 m elevation, a confining clay layer at a few meters' depth is noted with groundwater and geotechnical studies (Thiros, 2003; Leeflang, 2008), suppressing the depth to the 1,500 m/s contour. This observation is consistent with water well 57-248 (position 500 m) along 800 South that shows static water levels at 3 m depth or at the 1000 m/s contour. Where modern stream deposits are mapped, both Vp and Vs show large velocity variations that are consistent with meandering stream deposits or soft sediment deformation. To the west of position 1500 m along 700 South and west of position 2000 m along 800 South, Vs is mostly consistent with soft Holocene lacustrine and marsh soils (NEHRP class E) in the upper 20 m. Here, there is consistency between our measured Vs and borehole Vs measurements (McDonald and Ashland, 2008; Figure 1).

Above about 1295 m elevation or east of position 2,000 m on both profiles, we observe an increase in both Vp and Vs (Figure 11). We attribute the increase in Vp below 10 m depth to represent a shallower water table. A water well near the data gap at 700 East (position 3050 m) shows static water levels matching the 1,500 m/s contour depth, consistent with an unconfined groundwater system. This places the boundary between confined to unconfined groundwater near position 2000 m where we note a distinct step in the 1,500 m/s Vp contour. We identify stiffer Vs soils east of position 2000 m, consistent with older (latest Pleistocene) strata above the 1295 m elevation Gilbert high stand.

Above an elevation of about 1310 m, or east of position 3,500 m (cross street 900 East) and west of the EBF, we observe slower Vp and faster Vs in the upper 10-20 m depth (Figure 11). We attribute the slower Vp to an increase in depth to water saturated sediments and to the presence of colluvium at the base of the EBF. The faster Vs or stiffer soils, is consistent with the Personious and Scott (1992) mapped change in lithology to reflect older (late Pleistocene) lake strata at higher basin elevations. Immediately to the west of the EBF, we observe a slower velocity Vp and Vs, consistent with the presence of alluvium, colluvium and lacustrine deposits. A narrow low Vp/Vs ratio within the faulted region suggests dry soft soil occupies the fault zone. In the footwall of the EBF at position 4000 m (cross street 1100 East), we observe Vp > 1,500 m/s at about 3 m depth. This Vp increase is consistent with groundwater springs mapped along the footwall of the fault (Mower and Van Horn, 1973; Figure 1) and that strata in the footwall portion of the EBF define a barrier to lateral groundwater flow. Between position 4500-4600 m, a sharp increase in Vs, coupled with a change in surface slope, is consistent with a mapped fault. Personious and Scott (1992) place a strand of the EBF close to this location (Figure 9).

Reflection image quality varies along these profiles due to laterally changing lithology and fluid properties, but key tectonic features are clear on both profiles 700 South and 800 South (Figure 11). First, we observe km-wavelength folded lake strata in the upper 300 m depth between positions 2000-3500. The crest of one anticline is located between position 2500-3000 m (near cross street 500 East) where an artesian spring is located along 800 South. Here, high Vp is consistent with saturated sediments rising to the land surface elevation (refraction velocities in the upper 5 m are poorly resolved). Offset reflectors within this broad zone of folding is consistent with a distributed zone of shortening and faulting to the west of the EBF (Figure 9). Father west, reflection data quality suffers,

likely from the depth increase in saturated sediment and laterally changing near surface lithologies. However, reflector truncations and changing reflector dips are clear and consistent with faulting beneath the downtown SLC corridor. Of particular interest are the faults identified along strike of the WSF at the Salt Palace and along a CPT survey (between cross streets 200West and State Street). We suggest that the WSF extends through downtown SLC as a broad zone of faulting. Connecting 400 South CPT survey with the 500 South, 700 South and 800 South seismic profiles, we identify a northwest trend in the fold axis, parallel to local surface topography, parallel to the southern portions of the EBF and parallel to the top of Tertiary gravity signature (Figures 1, 2, and 3). The broad zone of folded strata is consistent with differential slip between the Warm Springs and EBFs, with a higher slip rate along the EBF compared to the WSF at this latitude.

A decrease in reflection imaging depths appears along the western portions of the profile that we relate to slower Vp and Vs values, a lower Vp/Vs ratio, and higher mode surface waves (best seen as Vs inversions). Wells that extend to a few hundred meters' depth, coupled with our gravity models, suggest that these folded and faulted strata are late Quaternary. This suggests that these faults may still be active, placing a higher seismic hazard for the downtown corridor than currently recognized.

Near 1000 East, we identify a prominent low Vp zone as colluvium related to sediments infilling in the hanging wall of the EBF (Figure 11). Reflectors beneath this colluvial wedge are folded over the EBF, with a 40 m offset along the shallowest reflector. This interpretation of draped strata within the EBF zone are consistent with the monoclonal warping documented in the nearby Dresden Place trenches by Machette (1992). A synclinal inflection in reflectors at position 4500 m (best seen on 800 South), are consistent with an additional strand of the EBF, as mapped by Personious and Scott (1992).

200 West

In 2017, we acquired a 700 m long north to south profile along 200 West, between 400 South and 100 South (Figure 3). The profile was acquired upon fan alluvium and Holocene lacustrine deposits, with a decrease in slope of 10 m from north to south. The Salt Palace is located immediately to the east of positions 0-200 m where lateral spread deposits and faulting has been interpreted.

Low velocity (<500 m/s) Vp is noted in the upper 3-5 m, consistent with mapped fan alluvium. This layer thins to the south where Holocene lacustrine deposits are mapped (Personious and Scott, 1992). The depth to Vp=1,500 m/s is highly variable and ranges in depth from 10-20 m. This variability is consistent with laterally changing lithologies and fluid properties. Vs values along the northern portions of the profile represent D-class soils. Beneath the southern portion of the profile, E-class soils are mapped. An abrupt termination in D3 soils are noted at position 350 m. The stiffer soils are consistent with soils mapped to the east of 200 West along the 200 South profile, or where lateral spread deposits are mapped.

The reflection profile (shown in depth converted with a 1-D model), shows considerable variability across the profile. Relatively flat lying strata are truncated and offset, consistent with faulting across the central portion of the profile. Where these truncations in reflectors are noted, we observe lateral

changes in Vp and Vs. A detailed velocity analysis and 2-D depth conversion is needed on this profile to separate velocity pull ups from laterally changing shallow Vp. Regardless, we identify faults that offset strata at less than 20 m depth. These faults are adjacent to the Salt Palace

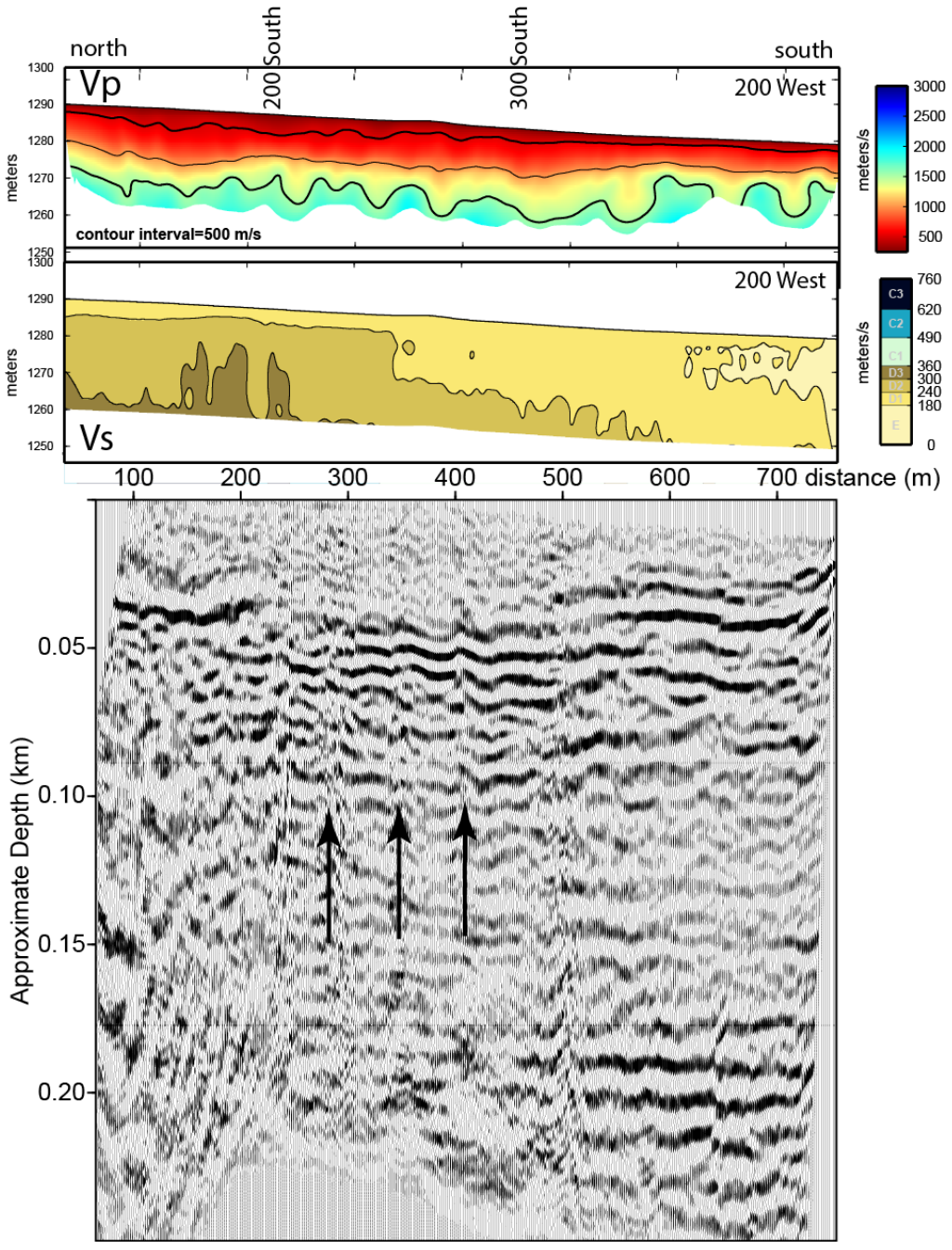

Figure 12. Vp, Vs and reflection results for the 200 West profile. Note the change in reflector quality across the profile.

400East/D Street transect

The 1.8 km long south to north 400 East seismic profile (Figures 1 and 3) highlights the seismic character and physical properties across the Salt Lake basin as we transition from low to high elevation, from fine (offshore) to courser grained (near shore), and from younger to older lacustrine deposits and alluvial deposits (Figure 3; Personious and Scott, 1992). This 2017 profile begins on lacustrine, marsh and alluvial deposits related to paleo lake Bonneville and terminates above lacustrine gravel and sand deposits related to a regressive lake phase (Personious and Scott, 1992). There is a data gap where the profile crosses a light rail line at 400 South; and 400 East crosses seismic profiles along 700 South at position 160 m, 500 South at position 610 m and 200 South at position 1310 m. The elevation rises from 1298 m at the south end of the profile to 1320 m at the northern end of the profile, between Gilbert and Provo high stands. The source to near geophone offset was 10 m for this profile.

At low elevations along the southern portions of the profile, shot gathers show relatively fast head wave seismic velocities (1,500-2200 m/s) beyond about 20 m source-geophone offset (Figure 5a and 5b). At higher elevations, this refractor appears at greater offsets, consistent with slower near surface velocities. Rayleigh wave velocities with respect to frequency progressively increase from south to north. For example, the 20 Hz Rayleigh wave phase velocity increases from about 180 m/s to 250 m/s across the profile. At lower frequencies (greater probing depths), this phase velocity contrast is greater. When a spiking deconvolution and bandpass filter is applied to the shot gathers, high quality reflections are observed on the southern shot gathers to more than 0.3 s two-way travel time (about 250 m depth) and little coherent reflection signal is observed below about 0.15 s two-way travel time (about 100 m depth) on shot gathers along the northern portions of the profile.

The top panel of Figure 13 represents Vp results to 20-40 m depth for the 400 East profile. Seismic head waves dive to greater depths in the presence of large velocity gradients, thus Vp imaging depths increases along the northern portions of the profile. A number of water wells have been drilled in the vicinity of this profile. Drillers logs to the south of the light rail data gap show sands and silts to the maximum drill depth of 200 m depth, and all show a water table that ranges from 7-9 m depth. Wells located to the north of the data gap all record water table to significantly greater depths. Between position 1100-1200 m (at an elevation of about 1,308 m), we observe a 9 m step down to the north along the 1,500 m/s contour, consistent with a relatively abrupt decrease in water table elevation at a mapped lithology boundary that represents a change from Qlam to regressive lake deposits (Personious and Scott, 1992). A second smaller step down along the 1,500 m/s contour is noted at position 1450 m. Vp above the water table ranges from about 400-1500 m/s, consistent with dry sands and silts noted on drillers logs (http://www.waterrights.utah.gov/wellinfo/wellsearch.asp). Vp values below the water table range from 1500-2500 m/s, consistent with saturated late Quaternary lake sediments. We exceed 2,450 m/s along the deepest part of the northern portion of this profile, consistent with Tertiary strata located below 30-35 m below land surface to the north of position 1500 m.

Vs derived from Rayleigh wave inversions show mostly NEHRP D1/D2-class stiff soils (180-300 m/s) across the southern portions of the profile in the upper 25 m (Figure 13). In general, there is a gradual increase in Vs from south to north, consistent with an increase in grain size or a transition from loose to stiff soils toward the basin margin. North of about position 1250 m, Vs increases abruptly to more than 300 m/s below a few meters' depth. This boundary coincides with the location of mapped lateral spread deposits (Qml) of Van Horn (1982) (Figure 1). From liquefaction, a rearrangement of grains into a denser packing structure decreases porosity by increasing soil density (e.g., Obermeier, 1996); thus an increase in soil stiffness or increased Vs compared to in situ strata. This Vs increase appears at a depth of a few meters below land surface, and assuming these deposits resulted from earthquake ground shaking, suggest a late Pleistocene earthquake was responsible for liquefaction at this site. A second abrupt increase in Vs appears about position 1600 m, with NEHRP C-class dense soils below about 10 m depth. This boundary is coincident with the transition from mapped lateral spread deposits to regressive sediments of the older Provo phase of lake Bonneville (18-15 ka). About 800 m to the west of this profile, at 1,317 m elevation, NEHRP B-Class (>760 m/s) rock was noted at a depth of 48 m (Tinsley et al., 1991). This is consistent with our refraction model that places Vp>2,450 m/s Tertiary rock at a similar depth. Although a step in Vs is observed at this boundary, we do not interpret this as a fault because the seismic reflection profile shows consistent dips and continuous reflectivity across this boundary.

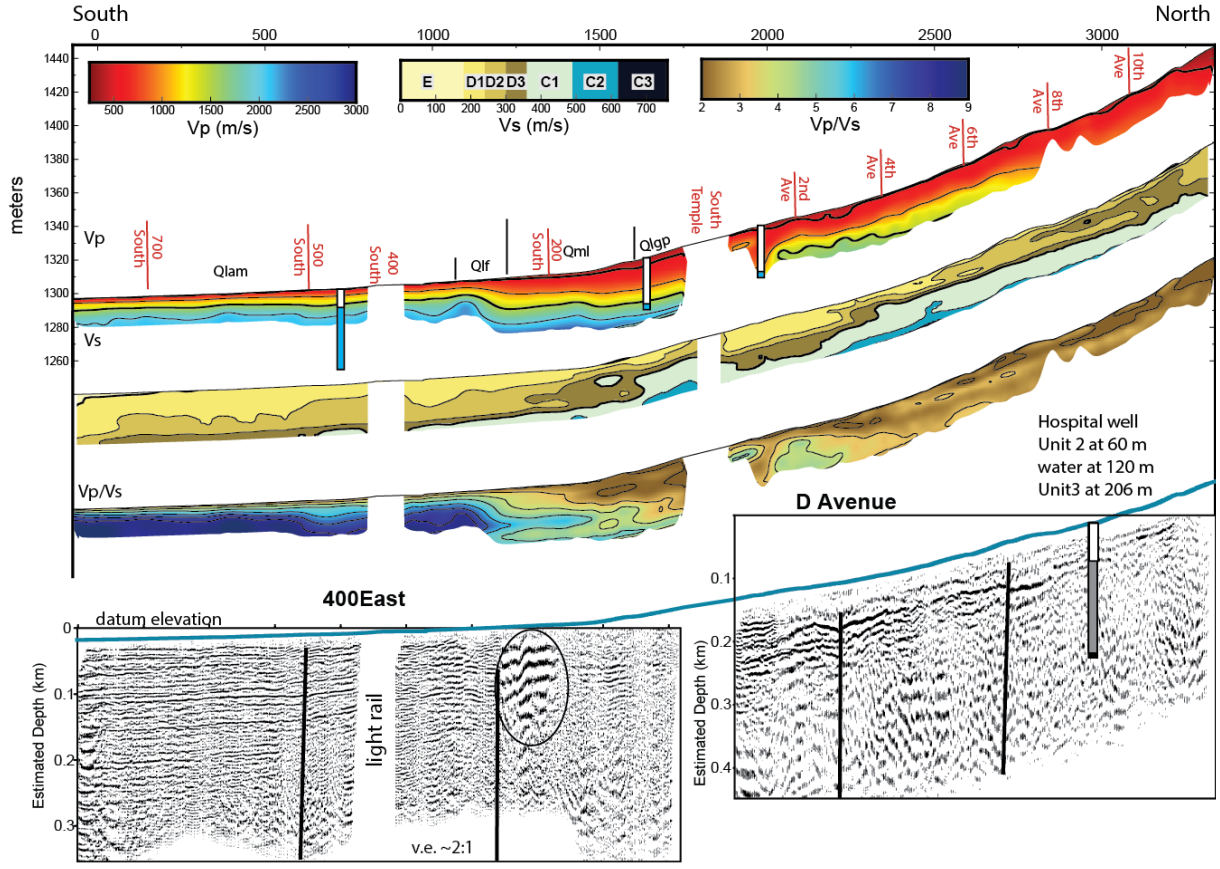

Figure 13. Vp, Vs, Vs30, Vp/Vs and reflection results for 400 East/D Street profile.

The 400 East seismic reflection profile shows near flat-lying strata along the southern 1200 m of the profile with a slight inflection of strata at position 650 m, close to the crossing of our profile along 500 South (Figure 13). Here, there is a slight decrease in Vp and an increase in Vs to the north of this presumed fault or axial surface. Between position 650 -1000 m, the strata dip about 4 degrees to the south. North of position 1,000 m, the reflectors gently roll over to form a ~200 m wide gentle fold. North of position 1,200 m, the seismic character changes considerably where the depth to water saturated sediments (Vp>1,500 m/s) increases and the stiffness in soils above the water table increases (increased Vp/Vs ratio). Although reflectors are observed along the northern portions of the profile, poor reflection quality preclude a detailed stratigraphic or structural interpretation. Within this higher elevation environment, we cannot confidently identify a fault that controls near surface velocity contrasts, but the folded strata that terminate at position 1,200 m, the step down in water table elevation to the north, and Tertiary strata identified at 30-40 m depth to the north are all consistent with an underlying fault that controls these near surface properties. The presence of lateral spread deposits along the xx degree sloping land surface slope deposits and the location adjacent to a presumed fault suggests that the lateral spread deposits are related to faults that underlie the near surface. Note that the depth to water saturated sediments is about 20 m depth at this location, significantly reducing the chance of further liquefaction from ground shaking (e.g., Obermeier, 1996). This suggests that the presumed earthquake that produced lateral spread deposits at this site occurred after the deposition of latest Pleistocene Lake Bonneville deposits while the groundwater elevations were likely shallower.

K Street profile

The 2017 1.5 km long north to south K Street seismic profile (Figure 1 and 3) extends across the Avenues District of SLC, with an increase in elevation of 150 m. This profile lies above Pleistocene deposits related to paleo lake Bonneville and post-Bonneville fan alluvium (Personious and Scott, 1992). The northern 200 m of the profile crosses the Provo high stand (Figure 1 and 3).

Vp in the upper few meters is generally greater than 500 m/s, consistent with little fan alluvium (Figure 14). Vp at our imaging limits does not exceed 1,500 m/s, consistent with a water table greater than 20 m depth (Figure 14). Lateral changes in Vp are noted near the 6th Ave, 8th Ave, and 10th Ave crossings. The 8th Ave crossing is coincident with the mapped change from lake deposits to alluvium, but shallow VP does not show a measurable change. Vs for the upper 10 m is mostly D-class stiff soils, and C-class dense soil is mapped between 10-30 m depth.

The reflection profile shows south-dipping reflectors in the upper ~100 -200m depth (Figure 14). A high amplitude reflector at shallow depths near the northern limits of this profile is consistent with top of Tertiary. We follow this reflector across several lateral truncations until the depth exceeds our imaging capabilities near position 750 m. We identify several faults, based on these truncations. We confidently identify these offsets along the top of Tertiary reflector, consistent with post-Neogene fault motion.

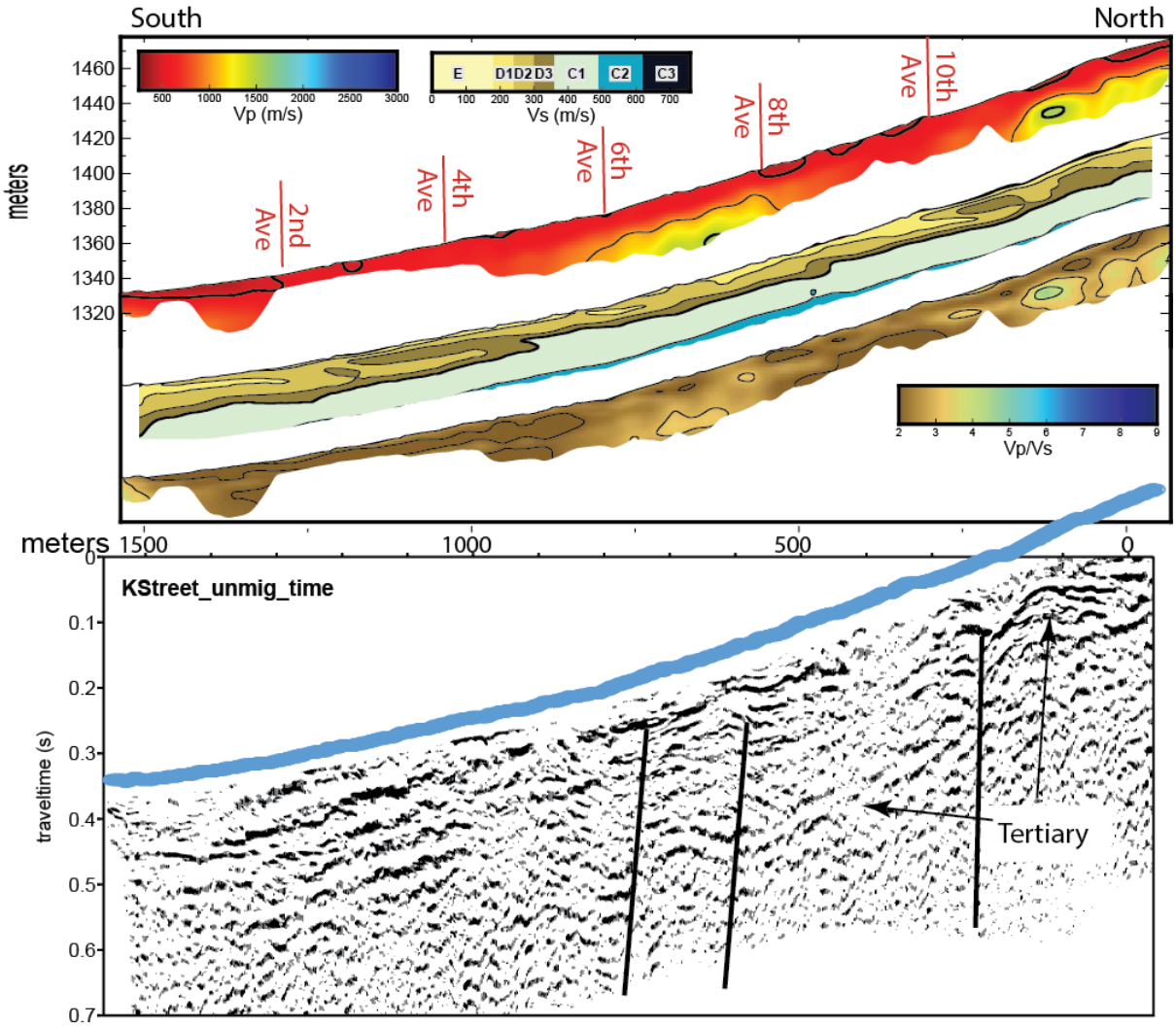

Figure 14. Vp, Vs, Vs30, Vp/Vs and reflection results for K Street profile.

1100 East/Cemetery transect

The south to north 1.6 km long 1100 East profile extends from 500 South to 4th Ave along both 1100 East and Q Street (Figures 1 and 3). Stepping west by a few meters, the 0.7 km Cemetery profile extends north to the slope break of the Salt Lake salient along Center Street. Personious and Scott (1992) mapped Pleistocene lacustrine deposits on the footwall side of the EBF, from the start of profile to position 400 m (Figure 15). Here, the land surface slopes to the northwest about 4 degrees. From position 400 m, where the EBF is mapped, to the northern transect termination, upwards of 10 m of middle Holocene to uppermost Pleistocene fan alluvium sits upon Pleistocene lake sediments. The surface slope increases from about 2-8 degrees along the northern 2 km of the profile. Tertiary strata are mapped approximately 300 m north of the cemetery.

We identify Vp values less than 500 m/s along the central and northern portions of the transect, to depths upwards of 10 m (Figure 15). We interpret these slow velocities to represent fan alluvium. At position 800 m (near cross street 100 South), we observe an abrupt step in the 1,500 m/s contour where depths to the presumed water table are at least 10 m deeper to the north. This change in depth is poorly constrained by refraction tomography, as imaging depths are limited to the north on the truncation. A step of about 5 m depth at the 1,500 m/s contour is noted at the mapped EBF. Vp progressively increases in velocity from position 1000 m-1750 m, then we observe an abrupt step down to the north along the 1,000 m/s contour. At the very northern end of the transect, Vp approaches 3,000 m/s, consistent with the presence of Tertiary strata below 20 m depth. Vs is dominated by D-class soils in the upper 10-15 m and C-class soils below. E-class soils are found at the base of the steep slope associated with the EBF, consistent with colluvium that builds at the steep slope base.

Seismic reflection data quality is highly variable along the 1100 East portion of the transect (Figure 15). We observe south and north dipping discontinuous reflectors within the footwall portion of the EBF, consistent with a zone of distributed faulting. This reflection pattern continues to position 850 m where reflectivity is mostly absent to the north. We interpret this abrupt termination in reflectivity to represent a step down in the EBF. This extends the fault approximately 450 m north of the Personious and Scott (1992) mapped location (Figure 15). Along the Cemetery/Center Street portion of the transect, we observe south-dipping strata with reflector truncations at positions 1800 m and 2100 m. These truncations are co-located with lateral changes in Vp. We interpret these lateral changes as strands of the Virginia Street fault that is mapped to the north of the profile termination. It is unclear the latest fault motion on the Virginia Street fault, but offsets in shallow strata and a step in the water table support late Quaternary fault motion. Thus, we extend strands of the Virginia Street fault to the south and beneath the Avenues district of SLC.

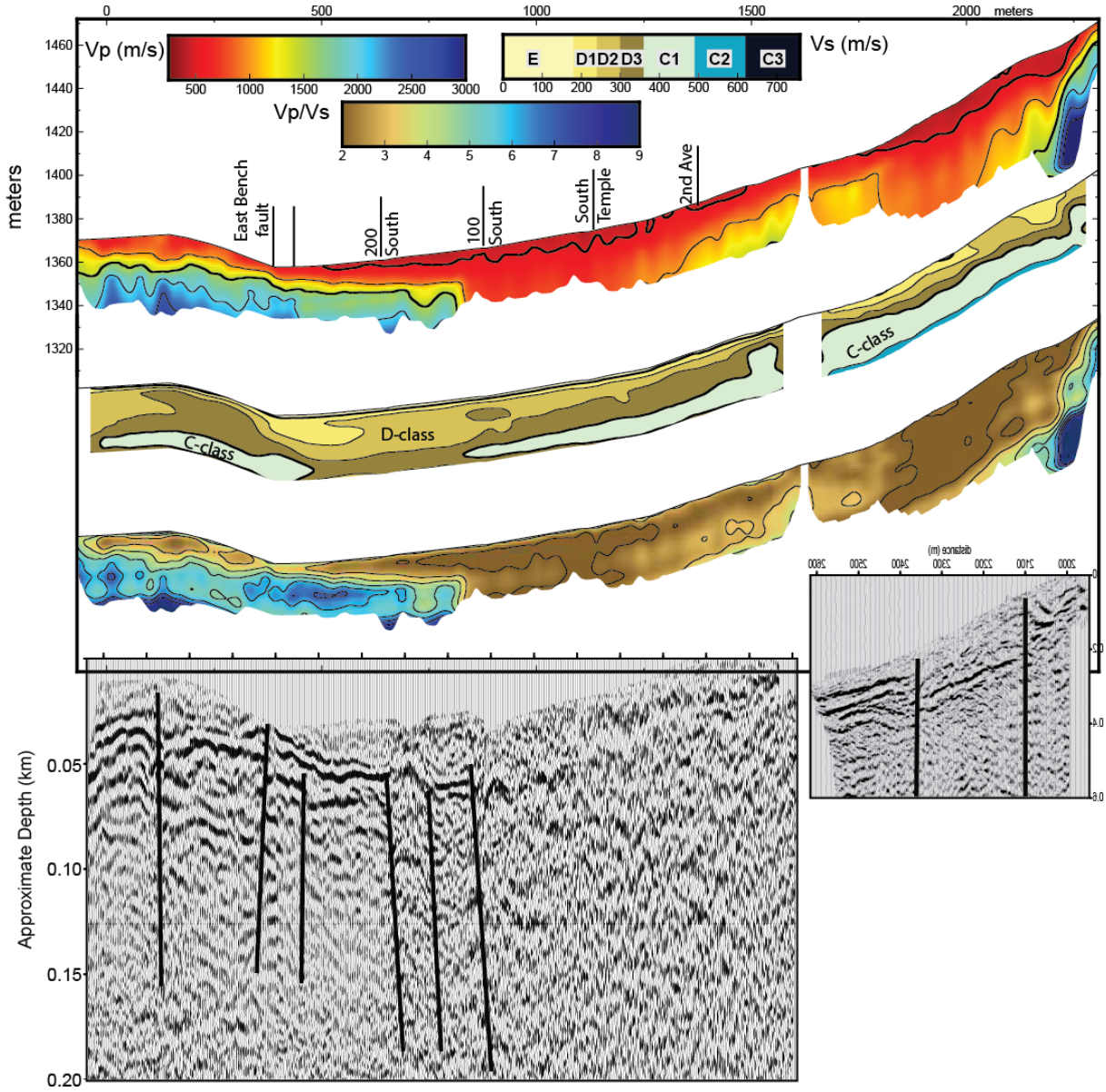

Figure 15. Vp, Vs, Vs30, Vp/Vs and reflection results for 1100 East/Cemetery transect.

Wolcott Street profile

The 2017 Wolcott Street profile is located 500 m west of the Penrose trench at the northern end of the EBF (Figure 1 and 3), where latest Pleistocene and Holocene vertical slip rates are estimated at 0.5–0.9 mm/yr. Along the seismic profile, no topographic scarp marks the fault at position 150 m (Figure 16). Near the northern portion of the profile, a steep topographic slope (at a bend in the profile) is related to alluvial fan development.

On the Vp profile, we add contours at 100 m/s because of the slow measured velocities. Vp < 500 m/s is noted in the upper 5 m between positions 150 m to the end of profile (Figure 16). These slow velocities are related to colluvium or alluvium. The fastest Vp that we measure is less than 1,000 m/s, consistent with the water table exceeding the imaging depths of our refraction survey. At the location of the mapped EBF, we not a 6-8 m step down to the north along the 600 m/s contour. A similar step down to the north along the Vs profile appears at the same location, consistent with changing lithologies across the EBF. Here, the top of NEHRP C-class soils steps down about 10 m. These velocities are consistent with late Pleistocene deposits. Assuming an age of 20 ka for the top of C-class Bonneville sediments, we place a slip rate of 0.5 mm/yr, consistent with slip estimates at the Penrose trench.

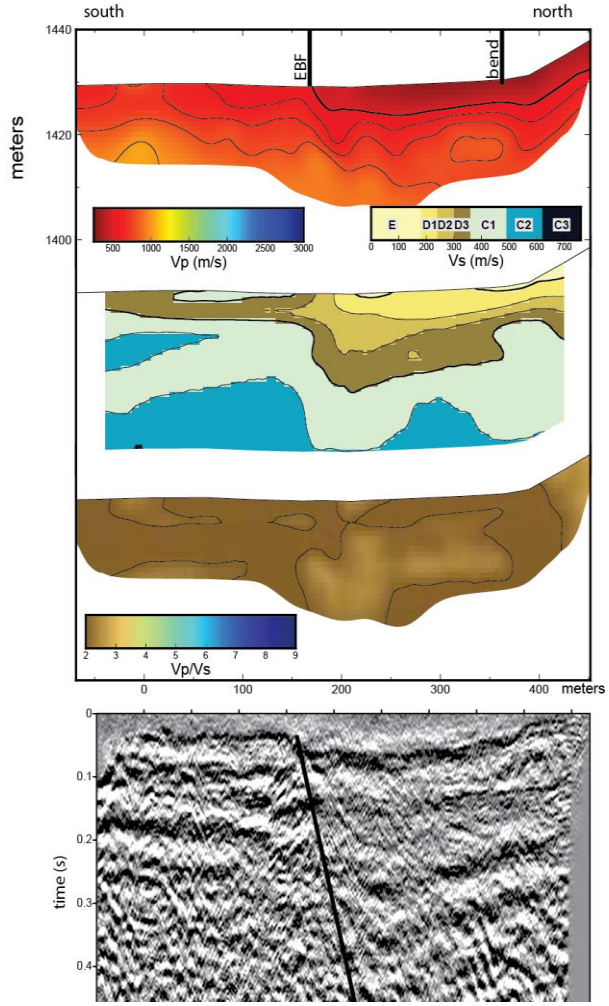

Figure 16. Vp, Vs, Vs30, Vp/Vs and reflection results for the Wolcott profile.

The reflection profile along Wolcott Street (Figure 15) shows down to the north step in a reflector in the upper 20 m, and an increase in reflector offsets at greater depths. This reflection pattern is consistent with growth faulting associated with the EBF.

Discussion

Faulting and folding beneath Salt Lake City

Whereas other reports have speculated about faults that lie beneath SLC, we present evidence that both faulting and folding is pervasive beneath the urban corridor. Additionally, we show that lateral spread deposits appear at a number of locales, and that these deposits are rooted in active faults. Gravity data show a clear signature associated with the WSF, and while more diffuse, this lateral density contrast continues to the south beyond the mapped extent of the fault and beneath downtown SLC. We map a prominent N20W-trending fold and related faults between 800 South and North Temple Street that parallels: 1) the surface topography (Figure 1 and 3); 2) the southern portions of the EBF (Figure 1); 3) the top of Tertiary gravity signature (Figure 2); and 4) the eastern boundary of seasonal groundwater subsidence derived from InSAR results (Hu et al, 2018; Figure 1). The broad zone of folded and faulted strata is consistent with differential slip between the Warm Springs and EBFs, with a higher slip rate along the EBF compared to the WSF at this latitude. High-resolution marine data in southern Utah Lake (Baskin and Berryhill, 1998) and the Great Salt Lake (Colman et al., 2002) map distributed zones of faulting within the basin. Here, we show that distributed faulting extends throughout the Salt Lake basin. We show evidence for overlap between fault segments of the Wasatch fault and that a large earthquake that initiates on either the WSF or EBF could also activate faults that surface beneath downtown SLC. The presence of low velocity sediments, a shallow water table, and paleo-liquefaction evidence suggests that portions of downtown SLC are at significant risk to earthquake ground amplification, faulting and liquefaction.

The EBF shows a clear topographic and seismic expression from the University of Utah campus, south to at 800 South. The results of this study point to a refined fault strand loactions along 200 South, 1100 East, 700 South and 800 South. The reflection results point to folded and offset strata. Specifically, results along 700 South and 800 South point to well-developed colluvium in the hanging wall of the fault and monoclonal warping similar to what was documented in the nearby Dresden Place trenches by Machette (1992). Reflector and Vp truncations along 1100 East and 200 South point to an additional fault strand that lies to the west of the mapped EBF.

We find an alignment of reflector truncations and changing Vp/Vs along a trend that parallels the Virginia Street fault. It is unclear the slip history of this fault, but we identify offsets as shallow as 20 m depth, consistent with late Pleistocene or later motion. Reflection data quality in the Avenues District of SLC produced low quality seismic reflection results due to shallow heterogeneities and greater depths to ground water.

Shallow fluid and soil properties

Water table

Vp profiles show distributions of soil and fluid properties beneath SLC. The most prominent Vp signature within the upper ~30 m represents the change from dry to water saturated sediments. We show evidence for confined and unconfined ground water systems and both shallow (less than a few m depth) and very deep groundwater systems. We show evidence that the EBF, near the southern portions of our study area, is a barrier to lateral groundwater flow and an artesian spring along 800 South (Figure 9) is located along the axis of a broad anticline. Other lateral steps in the 1,500 m/s contour that we tie to faulting suggest a strong tie between tectonics and groundwater systems. A newly published paper by Hu et al (2018) support this observation by showing differential subsidence and uplift along the presumed faults of the Salt Lake basin (Figure 1). Of particular interest to this study is that confined groundwater areas suggest confining pressures may be high. Coupled with low Vs in the upper 20 m, these zones point to areas that are prone to liquefy during an earthquake.

Colluvium and alluvium

Shallow, slow Vp (<500 m/s) is found at the base of steep slopes. Of particular interest is the wedge of low Vp at the base of the EBF along 200 South, 700 South, and 800 South (Figures 8 and 11). These colluvial wedges accumulate sediment at the base of a fault scarp following a surface rupturing earthquake. The thickness of these colluvial wedges suggest many surface rupturing earthquakes across the EBF. The wedges are a characteristic geological signature of normal fault earthquakes (McCalpin 1996), and if cored, drilled, or trenched, may be useful to determine earthquake recurrence by radio-carbon dating. Low velocity zones are also noted at the base of the WSF in North SLC (Figure 6), especially below notable slope breaks. However, these low velocity wedges are not as well developed along the WSF when compared to the EBF transects.

Other low velocity shallow zones can be correlated with fan alluvium near the basin margins throughout SLC. These slow velocities can be used to estimate the thickness of fan alluvium that post-dates Lake Bonneville. Shallow lake deposits that are mapped at the land surface (Personious and Scott, 1992) typically record faster Vp that is a result of better grain size packing and increased saturation.

Paleoliquefaction/lateral spread distributions

Earthquake induced liquefaction can produce significant damage to buildings when soft soil interacts with groundwater and loses its shear strength (e.g., Obermeier, 1996). Liquefaction typically occurs in the upper 10-15 m depth and evidence for past liquefaction events are noted throughout the SLC area. Groundwater must be present within the upper 10-15 m, but where high confining pressure and perched groundwater systems are found, these areas can also be at risk. Seasonal variations in

groundwater places the Salt Lake valley at greater risk to liquefaction during wetter spring (recharge) months when groundwater elevations increase (e.g., Thiros, 2003).

We show a strong correlation between measured Rayleigh wave velocities, calculated Vs, and mapped lateral spread deposits (see Figure 10 for 500 South example). We see anomalously fast Rayleigh wave signals along North Temple, 200 South, 500 South, 200 West and 400 East profiles and when we invert for Vs, we observe velocity inversions below 10 m depth. The Vs distributions on some profiles suggest a narrow pipe of high Vs material at 10-15 m depth, spreading out to a broader zone at shallower depths (500 South, North Temple). Anomalous Vs extends as shallow as 3 m beneath the road surface on many profiles. Given that the upper 1-2 m was likely disturbed during road construction, we suggest that ground disturbances extend to within a few meters below the surface on some profiles (e.g., 500 South). This observation is consistent with the Osmond et al (1965) report that showed the top of deformed strata at 2 m depth beneath the Hall of Justice site at 500 South and 300 East. Whereas NEHRP Class D2 soils highlight lateral spread deposits along 500 South, NEHRP Class C1 (dense soil) surrounds NEHRP Class D3 (stiff soil) along the North Temple and 400 East profiles. Additionally, the high velocity deposits appear to be buried at greater depths along the 400 East profile where water table depths exceed 10 m. This implies paleo-liquefaction events of differing ages may be common throughout SLC.

We use the seismic profile along 500 South to highlight paleo-liquefaction features. On Figure 17, we show the 500 South Vs and reflection profile, with the 1,500 m/s Vp (water table) contour, and depths to key stratigraphic boundaries superimposed on the Vs image. We show a 350 m wide zone of NEHRP Class D2 stiff soils surrounded by NEHRP Class-D1 looser soils between 3-10 m depth. This is consistent with the mapped lateral spread deposits of Personious and Scott (1992). We extract the stratigraphic boundaries from the Leeflang (2008) study, where we match the surface elevation from CPT measurements at the location of mapped lateral spread deposits. We note that the contact between upper Bonneville/post lake deposits of mostly silt and clay over lower Bonneville (upper Pleistocene) sand and gravel deposits. Pre-Bonneville deposits include interbedded alluvial gravels and silt. This report emphasized that the depth to these boundaries varied considerably in both trench and CPT studies. They conclude that the layers most likely to liquefy reside within the upper Bonneville unit.

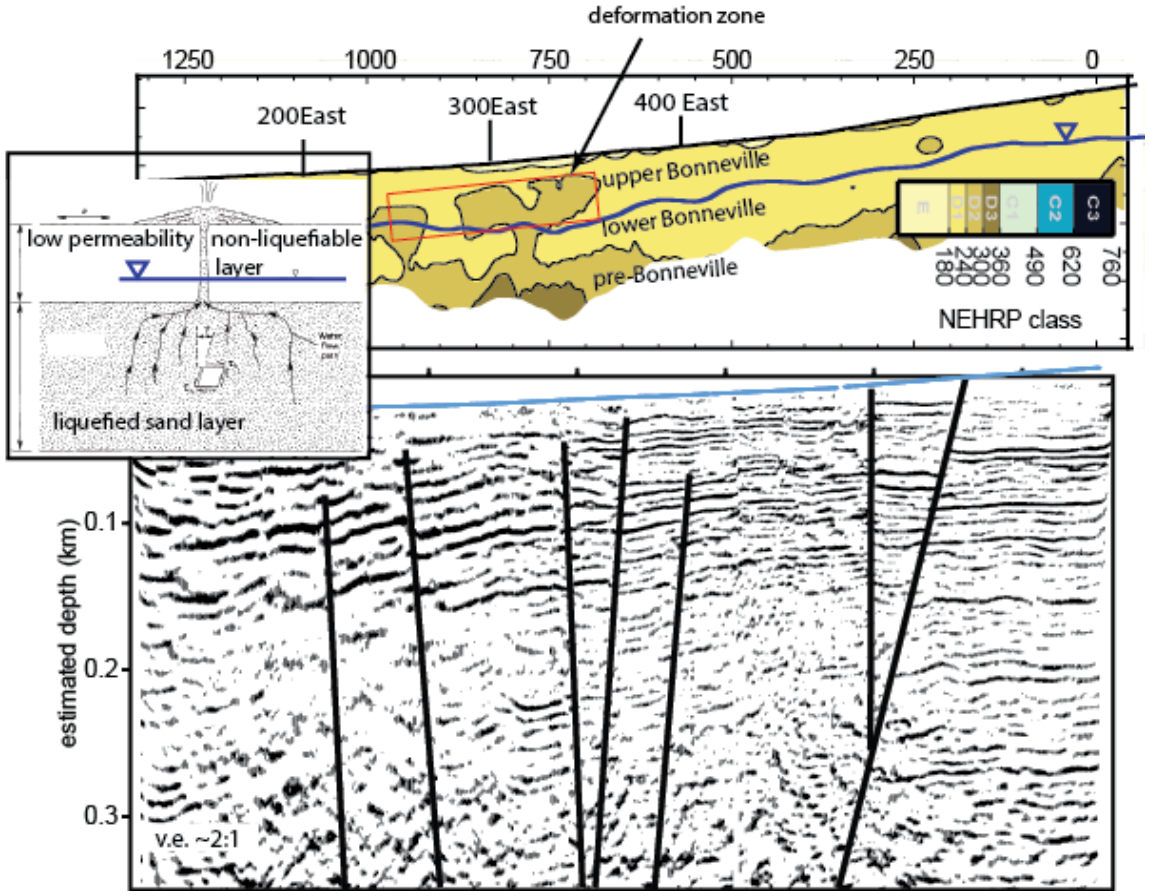

Figure 17. 500 South Vs and reflection profile with water table contour derived from Vp, and lithologic contacts derived from Osmond et al (1965) and Leeflang (2008). The width of the deformation zone corresponds to the extent of mapped lateral spread deposits from Personious and Scott (1992). Inset map from Obermeier (1996) showing the anatomy of a sand blow where low permeability silts and clays overlie a liquefied sand layer.

Included within Figure 17, we show the anatomy of a sand blow (Obermeier, 1996) where a low permeability non-liquefiable layer overlies a sandy layer. In this example, the water table lies within the low permeability zone. We suggest this model is similar to our findings in that the pre-Bonneville coarse-grained materials liquefied during an earthquake and injected material upward through the low permeability upper Bonneville deposits. The pipe-like high velocity material that lies below the mapped lateral spread is consistent with the original Osmond et al (1965) report where the observe liquefaction dikes lie beneath differential settlement and compaction. This pattern of deformation is consistent with a Holocene earthquake that experienced ground shaking adequate to produce shallow deformation. Given that the deformation zone is rooted in faults, this may require a relatively low magnitude earthquake to generate liquefaction (e.g., Olson et al., 2005; Figure 18). This study compiled findings from a number of sites to sow that when the epicentral distance is within a few km of high liquefaction susceptibility area, an earthquake <M5 can induce liquefaction. Indeed, the M 4.5 Randolph earthquake, located in Northern Utah, generated liquefaction less than one km from the earthquake epicenter

(DuRoss and Pankow, 2010). Thus, given the location of Holocene faults beneath downtown SLC, we suggest that smaller magnitude earthquakes may place SLC at higher risk to liquefaction.

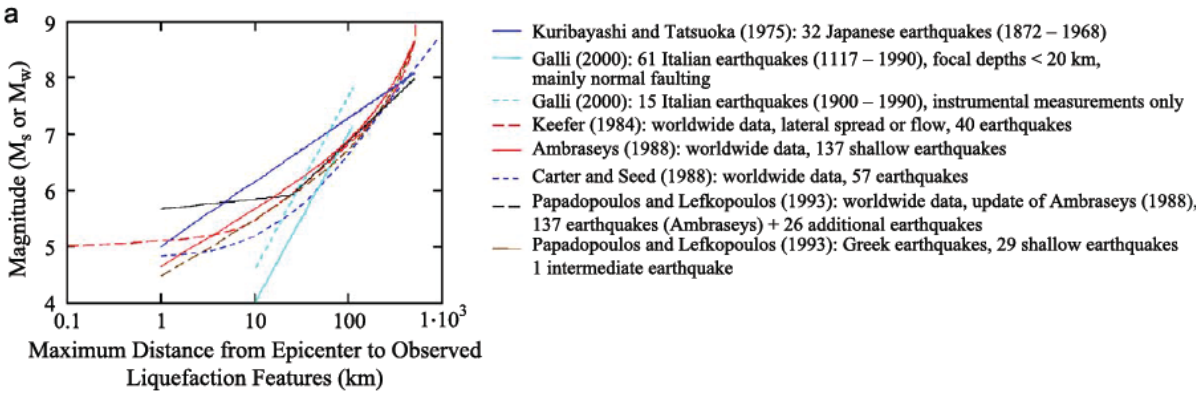

Figure 18. Earthquake epicentral distance to incur liquefaction compared to seismic moment magnitude (modified from Olson et al., 2005).

Seismic site amplification - Vs30 results

An important application of Vs is to predict site amplification of ground shaking during an earthquake. Many building codes require consideration of site response by using a time-averaged Vs to a depth of 30 m (VS30) (Borcherdt 2002; ICBO 1997). To assess the use of a seismic land streamer to measure Vs30, we compare our inversion results near three boreholes located along 700 South (Figure 1). Figure 19 shows the results of our inversion for five shots that surround the borehole measurements. The difference in methodology is that we rapidly acquire our data directly on a road surface, while the borehole measurements are in-situ and are time consuming to collect. We show comparable Vs measurements at these locations to about 25 m depth. At greater depths, our measurements tend to overestimate Vs. Where Vs increases, a similar analysis (well 121) shows that we slightly underestimate Vs30. However, because Vs30 is a time averaged approach, these differences have a minimal effect on Vs30 calculations. We conclude that our Vs30 measurements are within 5% of borehole-derived Vs values. Our five comparative measurements were collected in a few minutes, compared to a multi-hour campaign to acquire downhole Vs measurements.

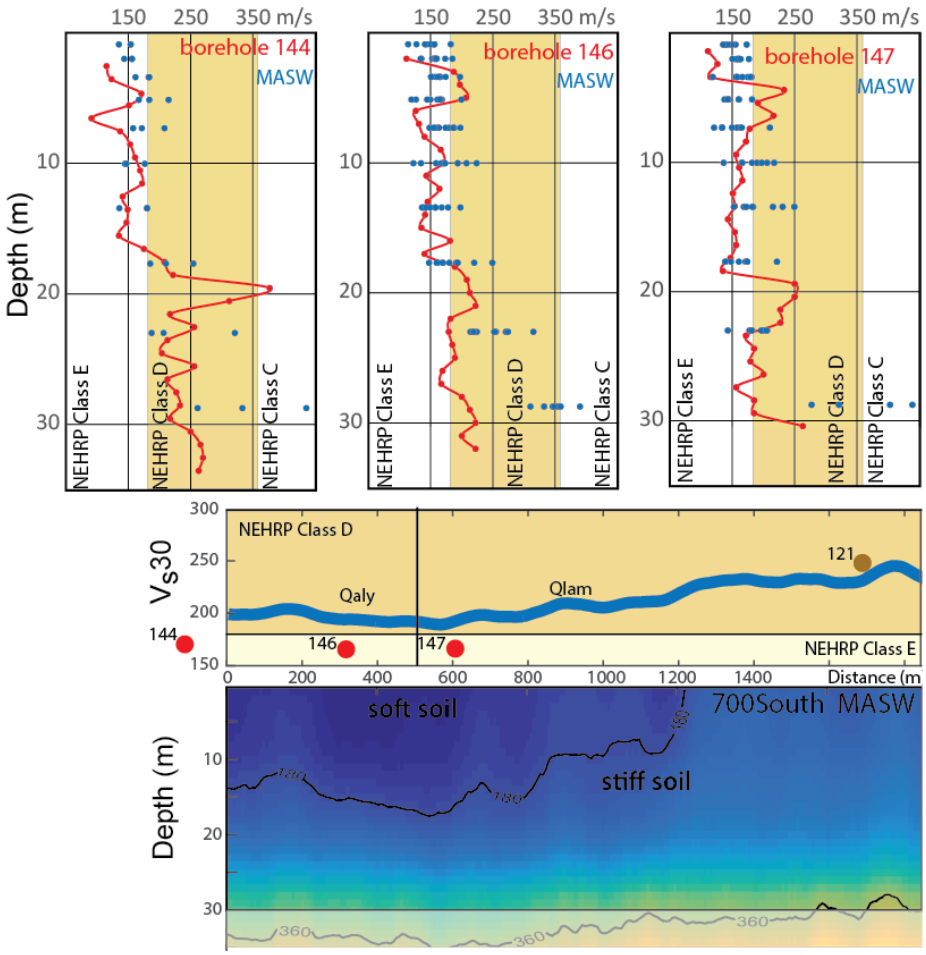

Figure 19. (top) Vs with depth for our results (blue dots) and borehole Vs measurements (red lines) from McDonald and Ashland (2008). Note the similar measurements in the upper 25 m. (bottom) Vs30 and Vs, in profile. Red dots represent borehole measurements. Note the slight overestimate of our results within low Vs zones (wells 144, 146, and 147) and an underestimate of our results in higher velocity areas (well 121).

Figure 20a shows a Vs30 map derived from our Vs inversions. Our results show a direct relationship between mapped lithologies/surface elevation and Vs30 values. Our results are comparable to downhole Vs point measurements (Figure 20b; McDonald and Ashland, 2008). Where Bonneville lake deposits are mapped, we observe low shear wave velocities (NEHRP Class E and D1 soft soils) and where alluvial fan deposits are mapped, generally NEHRP Class D2/D3 stiff soils are measured. Known fault locations of the WSF and EBF show soft rock (NEHRP Class C1) materials in the footwall block of the fault adjacent to NEHRP Class D soils in the hanging wall block. This product can be used to model site response for the SLC metropolitan area. Coupled with water table measurements, we can use this product to assess liquefaction susceptibility.

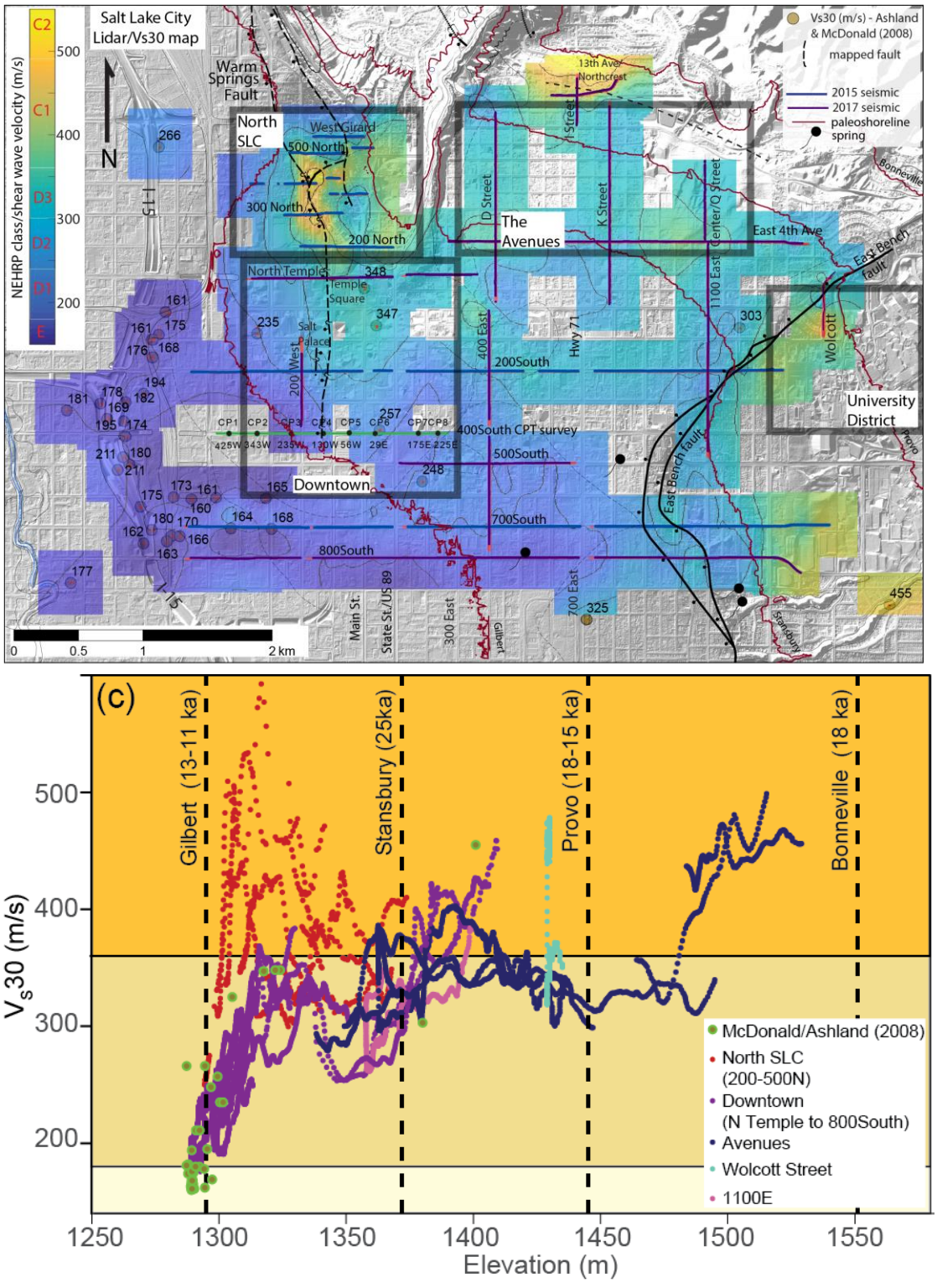

Figure 20. Vs30 map and Vs30 vs elevation.

From this database of 15,000 Vs profiles, we can examine the relationship between elevation, slope, lithology, and Vs30. Figure 20b shows that the Vs30/elevation relationship is not linear, but likely dependent on lithology, slope conditions and other factors. Further analysis will allow us to fully explore the relationship between Vs and surface properties.

Summary

Seismic imaging through SLC has produced a catalog of faults, soil properties and fluid distributions. We compare our seismic results to gravity models, paleoseismic trench studies, and geologic maps. Our imaging approach sheds light on numerous geologic processes that include hazards and resource assessments. Coupled with detailed field mapping, Lidar measurements, trench studies and regional surveys that include gravity modeling, we can advance our hazard assessments for the Salt Lake City urban corridor.

Data Archival

Seismic data are available immediately upon request from lliberty@boisestate.edu. Seismic field records will be archived at the Incorporated Research Institutions for Seismology (IRIS) as an assembled dataset (http://ds.iris.edu/ds/nodes/dmc/forms/assembled-id/) and data products will be archived at the Utah Geological Survey as a GeoData archive (http://geodata.geology.utah.gov). Archival will be submitted within one year of project completion (April 14, 2019).

References

Armstrong, P. A., Taylor, A. R., & Ehlers, T. A. (2004). Is the Wasatch fault footwall (Utah, United States) segmented over million-year time scales?. *Geology*, 32(5), 385-388.

Bartlett, S. F., and Alcorn, P. (2004). Estimation of preconsolidation stress and compression ratio from field and laboratory measurements from the I-15 reconstruction project, Salt Lake City, Utah (No. UT-03.20).

Bashore, W. M. (1982). Upper crustal structure of the Salt Lake Valley and the Wasatch fault from seismic modeling, M.S. Thesis, University of Utah, Salt Lake City.

Boore, D. M., & Atkinson, G. M. (2008). Ground-motion prediction equations for the average horizontal component of PGA, PGV, and 5%-damped PSA at spectral periods between 0.01 s and 10.0 s. Earthquake Spectra, 24(1), 99-138.

Borcherdt, R. D., 2002. Empirical evidence for site coefficients in building code provisions, Earthquake Spectra 18 (2), 189–217.

Bruhn, R., P. Gibler,W. Houghton, andW. Parry (1992). Structure of the Salt Lake segment, Wasatch normal fault zone: Implications for rupture propagation during normal faulting, in Assessment of Regional Earthquake Hazards and Risk along the Wasatch Front, Utah, U. S. Geol. Surv. Prof. Pap. 1500-A-J, pp. H1–H25.

Caine, J. S., Evans, J. P., & Forster, C. B. (1996). Fault zone architecture and permeability structure. Geology, 24(11), 1025-1028.

Catchings, R. D., Rymer, M. J., Goldman, M. R., Sickler, R. R., & Criley, C. J. (2014). A method and example of seismically imaging near-surface fault zones in geologically complex areas using Vp, Vs, and their ratios. Bulletin of the Seismological Society of America, 104(4), 1989-2006.

Chen, C. Y., & Maloof, A. C. (2017). Revisiting the deformed high shoreline of Lake Bonneville. Quaternary Science Reviews, 159, 169-189.

dePolo, C. M., D. G. Clark, D. B. Slemmons, and A. R. Ramelli (1991), Historical surface faulting in the Basin and Range Province, western North America: Implications for fault segmentation, J. Struct. Geol., 13(2), 123–136.

dePolo, C. M., D. G. Clark, D. B. Slemmons, and W. H. Aymard (1989). Historical Basin and Range Province surface faulting and fault segmentation, in Fault Segmentation and Controls of Rupture Initiation and Termination, Proceedings of Workshop XLV, D. P. Schwartz and R. H. Sibson (Editors), U.S. Geol. Surv. Open-File Rept. 89-315, 131–162.

DuRoss, C. B., and M. D. Hylland (2015), Synchronous ruptures along amajor graben-forming fault system—Wasatch and West Valley fault zones, Utah, USA, Bull. Seismol. Soc. Am., 105(1), 14–37, doi:10.1785/0120140064.

DuRoss, C.B., Hylland, M.D., McDonald, G.N., Crone, A.J., Personius, S.F., Gold, R.D., and Mahan, S.A., 2014, Holocene and latest Pleistocene paleoseismology of the Salt Lake City segment of the Wasatch fault zone, Utah, at the Penrose Drive trench site, in DuRoss, C.B. and Hylland, M.D., Evaluating surface faulting chronologies of graben-bounding faults in Salt Lake Valley, Utah—new paleoseismic data from the Salt Lake City segment of the Wasatch fault zone and the West Valley fault zone—Paleoseismology of Utah, Volume 24: Utah Geological Survey Special Study 149, p. 1–39, 6 appendices, 1 plate, CD.

DuRoss, C.B., and Pankow, K.L., 2010, Liquefaction in the 15 April 2010 Mw 4.5 Randolph, Utah, earthquake [abs.]: American Geophysical Union, Fall Meeting 2010, abstract #S51B-1931.

DuRoss, C. B., Personius, S. F., Crone, A. J., Olig, S. S., Hylland, M. D., Lund, W. R., & Schwartz, D. P. (2016). Fault segmentation: New concepts from the Wasatch fault zone, Utah, USA. Journal of Geophysical Research: Solid Earth, 121(2), 1131-1157.

Ehlers, T. A., Willett, S. D., Armstrong, P. A., & Chapman, D. S. (2003). Exhumation of the central Wasatch Mountains, Utah: 2. Thermokinematic model of exhumation, erosion, and thermochronometer interpretation. *Journal of Geophysical Research*: Solid Earth, 108(B3).

Gardner, G. H. F., Gardner, L. W., and Gregory, A. R. (1974). Formation velocity and density— The diagnostic basics for stratigraphic traps. Geophysics, 39(6), 770-780.

Gribler, G., Liberty, L. M., Mikesell, T. D., & Michaels, P. (2016). Isolating retrograde and prograde Rayleigh-wave modes using a polarity mute. *Geophysics*, 81(5), V379-V385.

Hill, J. (1988). A finite difference simulation of seismic wave propagation and resonance in Salt Lake Valley, Utah, M.S. Thesis, University of Utah, Salt Lake City, Utah.

Hill, J., Benz, H., Murphy, M., and Schuster, G. (1990). Propagation and resonance of SH waves in the Salt Lake Valley, Utah. Bulletin of the Seismological Society of America, 80(1), 23-42.

Hu, X., Lu, Z., & Wang, T. Characterization of Hydrogeological Properties in Salt Lake Valley, Utah Using InSAR. *Journal of Geophysical Research*: Earth Surface.

Hunter, J. A., Pullan, S. E., Burns, R. A., Gagne, R. M., & Good, R. L. (1984). Shallow seismic reflection mapping of the overburden-bedrock interface with the engineering seismograph—Some simple techniques. *Geophysics*, 49(8), 1381-1385.

International Council of Building Officials (ICBO), 2000. International Building Code, Falls Church, VA

IRIS DMC (2010), Data Services Products: EARS EarthScope Automated Receiver Survey, doi:10.17611/DP/EARS.1.

Kleinfelder, Inc. (1999). Geologic investigation, Salt Palace Expansion, Phase II,NWcorner 200 South andWest Temple, Salt Lake City, Utah, unpublished consultant report to Salt Lake County, 23 pp., available online at http://geodata.geology.utah.gov/pages/preview.php?ref=467 (last accessed July 2018).

Korbay, S. R., & McCormick, W. V. (1999). Faults, lateral spreading, and liquefaction features, Salt Palace Convention Center, Salt Lake City [abs.]: Association of Engineering Geologists. In 42nd Annual Meeting Program with Abstracts (p. 73).

Lee M.W. 2003. Velocity ratio and its application to predicting velocities. U.S. Geological Survey Bulletin. 2197, pp. 15.

Leeflang, B. A. (2008). Ground displacement investigations in downtown Salt Lake City, Utah, using the cone penetrometer, University of Utah M.S. thesis, Salt Lake City, 160 pp.

Liberty, L. (2011). Hammer seismic reflection imaging in an urban environment. The Leading Edge, 30(2), 146-153.

Liberty, L. M., and Gribler, G. (2014) Development of land streamer technologies for estimating shear wave velocities in an urban environment, US Geological Survey Final Technical Report, 21 p. https://earthquake.usgs.gov/cfusion/external_grants/reports/G13AP00032.pdf

Mabey, D.R. (1992). Subsurface geology along the Wasatch Front, in Assessment of Earthquake Hazards and Risk Along the Wasatch Front, Utah, P.L. Gori and W.W. Hays (Editors), U.S. Geol. Surv. Pro. Pap. 1500-A-J, C1-C16.

Machette, M. N., S. F. Personius, and A. R. Nelson (1992). Paleoseismology of the Wasatch fault zone: a summary of recent investigations, interpretations, and conclusions, in Assessment of Regional Earthquake Hazards and Risk along the Wasatch Front, Utah, P. L. Gori and W. W. Hays (Editors), U.S. Geol. Surv. Profess. Pap. 1500-A, A1–A71.

Mattson, A. (2004). Tomographic imaging of late quaternary faulting, Oquirrh Mountains, Utah. *Journal of Geophysical Research*: Solid Earth, 109(B11).

Mavko, G., Mukerji, T., & Dvorkin, J. (2009). The rock physics handbook: Tools for seismic analysis of porous media. Cambridge university press.

McDonald, G. N., & Ashland, F. X. (2008). Earthquake site conditions in the Wasatch Front urban corridor, Utah. Utah Geological Survey.
McKean, A. (2014). Interim geologic map of the Salt Lake City North quadrangle, Salt Lake and Davis Counties, Utah, contract deliverable to US Geological Survey NEHRP award G13AC00169, 43 p.
Morey, D., & Schuster, G. T. (1999). Palaeoseismicity of the Oquirrh fault, Utah from shallow seismic tomography. *Geophysical Journal International*, 138(1), 25-35.
Moser, T. J. (1991). Shortest path calculation of seismic rays. *Geophysics*, 56(1), 59-67.
Mower, R. W., & Van Horn, R. (1973). Map showing minimum depth to water in shallow aquifers (1963-72) in the Sugar House quadrangle. Salt Lake County, Utah: US Geological Survey Map I-766-I, scale, 1:24,000.
Obermeier, S. F. (1996). Use of liquefaction-induced features for paleoseismic analysis—an overview of how seismic liquefaction features can be distinguished from other features and how their regional distribution and properties of source sediment can be used to infer the location and strength of Holocene paleo-earthquakes. *Engineering Geology*, 44(1-4), 1-76.
Olsen, M. J., Bartlett, S. F., & Solomon, B. J. (2007). Lateral spread hazard mapping of the Northern Salt Lake Valley, Utah, for a M7. 0 scenario earthquake. Earthquake Spectra, 23(1), 95-113.
Olson, S. M., Green, R. A., & Obermeier, S. F. (2005). Geotechnical analysis of paleoseismic shaking using liquefaction features: a major updating. Engineering Geology, 76(3-4), 235-261.
Osmond, J. C., Hewitt, W. P., and Van Horn, R. V. (1965). "Engineering Implications and Geology, Hall of Justice Excavation, Salt Lake City, Utah," Utah Geological and Mineral Survey, Special Studies No. 11, 35 p.
Oviatt, C.G., 2015. Chronology of Lake Bonneville, 30,000 to 10,000 yr BP. Quat. Sci. Rev. 110, 166e171.
Oviatt, C.G., Currey, D.R., Sack, D., 1992. Radiocarbon chronology of Lake Bonneville, eastern Great Basin, USA. Palaeogeogr. Palaeoclimatol. Palaeoecol. 99, 225e241.
Personius, S.F. and W.E. Scott (1992). Surficial geologic map of the Salt Lake City segment and parts of adjacent segments of the Wasatch fault zone, Davis, Salt Lake, and Utah Counties, Utah, U.S. Geol. Surv. Misc. Inv. Series, Map I-2106, scale 1:50,000.
Petersen, M. D., Frankel, A. D., Harmsen, S. C., Mueller, C. S., Haller, K. M., Wheeler, R. L., ... & Luco, N. (2008). Documentation for the 2008 update of the United States national seismic hazard maps (No. 2008-1128). Geological Survey (US).
Price, D. (1985). Ground Water in Utah's Densely Populated Wasatch Front Area: The Challenge and the Choices. US Government Printing Office.
Radkins, H., M. Murphy, and G. Schuster (1989). Subsurface map and seismic risk analysis of the Salt Lake Valley, Utah Geological and Mineral Survey Report, Contract 5-24496.
Robison, R. M., and T. N. Burr (1991). Fault-rupture hazard analysis using trenching and borings: Warm Springs fault, Salt Lake City, Utah, in Proc. of the 27th Symposium on Engineering Geology and Geotechnical Engineering, J. P. McCalpin (Editor), Idaho Dept. of Trans., Boise, 26-1–26-13.
Roten, D., Olsen, K. B., Pechmann, J. C., Cruz-Atienza, V. M., and Magistrale, H. (2011). 3D simulations of M 7 earthquakes on the Wasatch fault, Utah, Part I: Long-period (0–1 Hz) ground motion. Bulletin of the Seismological Society of America, 101(5), 2045-2063.
Simon, D. B., and R. J. Shlemon (1999). The Holocene "Downtown fault" in Salt Lake City, Utah (abstract), Abstr. Programs Assoc. Eng. Geol. 85 pp.
Simon-Bymaster, Inc. (1999). Report of geologic investigation: Salt Palace Convention Center expansion project, 100 South West Temple Street,
Salt Lake City, Unpublished consultant report for Salt Lake County, 27 pp.
Stephenson, W. J., Louie, J. N., Pullammanappallil, S., Williams, R. A., & Odum, J. K. (2005). Blind shear-wave velocity comparison of ReMi and MASW results with boreholes to 200 m in Santa Clara

Valley: implications for earthquake ground-motion assessment. Bulletin of the Seismological Society of America, 95(6), 2506-2516.

Stephenson, W. J., Odum, J. K., Williams, R. A., McBride, J. H., & Tomlinson, I. (2012). Characterization of Intrabasin Faulting and Deformation for Earthquake Hazards in Southern Utah Valley, Utah, from High-Resolution Seismic Imaging. Bulletin of the Seismological Society of America, 102(2), 524-540.

Scott, W.E. and R.R. Shroba (1985). Surficial geologic map of an area along the Wasatch fault zone in the Salt Lake Valley, Utah, U.S. Geol. Surv. Open-File Report. 85-448, scale 1:24,000.

St. Clair, J. (2015). Geophysical investigations of underplating at the Middle American Trench, weathering in the critical zone, and snow water equivalent in seasonal snow, PhD thesis, Univ. of Wyoming.

Thiros, S. A. (2003). Hydrogeology of shallow basin-fill deposits in areas of Salt Lake Valley, Salt Lake County, Utah. US Department of the Interior, US Geological Survey Water-Resources Investigations Report 03-4029.

Tinsley, J. C., K. W. King, D. A. Trumm, D. L. Carver, and R. A. Williams (1991). Geologic aspects of shear-wave velocity and relative ground response in Salt Lake Valley, Utah, in Proceedings of the 27th Symposium on Engineering Geology & Geotechnical Engineering, J. P. McCalpin, (Editor), Pocatello, Idaho, 25-1 to 25-9.

Van der Veen, M. and Green, A.G., 1998. Land streamer for shallow data acquisition: evaluation of gimbal-mounted geophones. Geophysics, 63, 1408-1413.

Van der Veen, M. Spitzer, R., Green, A.G., and Wild, P., 2001. Design and application of a towed land-streamer for cost-effective 2D and pseudo-3D shallow seismic data acquisition. Geophysics, 66, 482-500.

Van Horn, R., 1982, Surficial geologic map of the Salt Lake City North quadrangle, Davis and Salt Lake Counties, Utah: U.S. Geological Survey Miscellaneous Investigations Series Map I-1404, 1 plate, scale 1:24,000.

Wills, C. J., Petersen, M., Bryant, W. A., Reichle, M., Saucedo, G. J., Tan, S. and Treiman, J. (2000). A site-conditions map for California based on geology and shear-wave velocity. Bulletin of the Seismological Society of America, 90(6B), S187-S208

Williams, R. A., King, K. W., & Tinsley, J. C. (1993). Site response estimates in Salt Lake Valley, Utah, from borehole seismic velocities. Bulletin of the Seismological Society of America, 83(3), 862-889.

Yilmaz, O. (2001). Seismic Data Analysis: Processing, Inversion, and Interpretation of Seismic Data, Society of Exploration Geophysicists, Tulsa IG#10 series, Oklahoma, 2027 pp.

Zelt, C. A., Haines, S., Powers, M. H., Sheehan, J., Rohdewald, S., Link, C., Hayashi, K., Zhao, D., Zhou, H., Burton, B. L., Petersen, U. K., Bonal, N. D., & Doll, W. E., 2013. Blind test of methods for obtaining 2-D near surface seismic velocity models from first-arrival traveltimes, Journal of Environmental and Engineering Geophysics, 18, 183-194, DOI:10.2113/JEEG18.3.183.